# MAPPING AND FUTURE PREDICTION OF LAND USE AND LAND COVER DYNAMICS USING GOOGLE EARTH ENGINE AND AN ARTIFICIAL NEURAL NETWORK MODEL IN THE JUCUSBAMBA RIVER BASIN, AMAZONAS (NW-PERU)

ZABALETA-SANTISTEBAN, J. A.[1*] – CACHAY-REYNAGA, R.[1] – ROJAS-BRICEÑO, N. B.[2] – SILVA-LÓPEZ, J. O.[3] – MEDINA-MEDINA, A. J.[1] – TUESTA-TRAUCO, K. M.[1] – RIVERA-FERNANDEZ, A. S.[1] – SÁNCHEZ-VEGA, J. A.[1] – SILVA-MELENDEZ, T. B.[1] – GRANDEZ-ALBERCA, M. A.[1] – SALAS-LÓPEZ, R.[1] – OLIVA-CRUZ, M.[1] – GÓMEZ-FERNÁNDEZ, D.[4] – BARBOZA, E.[1*]

*[1]Centro de Investigación en Geomática Ambiental (CIGA), Instituto de Investigación para el Desarrollo Sustentable de Ceja de Selva (INDES-CES), Universidad Nacional Toribio Rodríguez de Mendoza de Amazonas, Chachapoyas 01001, Peru*
*(e-mail: rodrich.rcr@gmail.com – Cachay-Reynaga, R.; angel.medina@untrm.edu.pe – Medina-Medina, A. J.; katerin.tuesta.epg@untrm.edu.pe – Tuesta-Trauco, K. M.; abner.rivera.epg@untrm.edu.pe – Rivera-Fernandez, A. S.; 7246207471@untrm.edu.pe – Sánchez-Vega, J. A.; 7680096361@untrm.edu.pe – Silva-Melendez, T. B.; marlen.grandez.epg@untrm.edu.pe – Grandez-Alberca, M. A.; rsalas@indes-ces.edu.pe – Salas López, R.; manuel.oliva@iuntrm.edu.pe – Oliva-Cruz, M.)*

*[2]Grupo de Investigación en Ciencia de la Información Geoespacial (CIGEO), Instituto de Investigación para el Desarrollo del Perú, Universidad Nacional de Moquegua, Pacocha 18610, Peru*
*(e-mail: nrojasb@unam.edu.pe)*

*[3]Área de cartografía y teledetección, Laboratorio de Agrostología, Instituto de Investigación en Ganadería y Biotecnología, Facultad de Ingeniería Zootecnista, Agronegocios y Biotecnología, Universidad Nacional Toribio Rodríguez de Mendoza de Amazonas, Chachapoyas 01001, Peru*
*(e-mail: jhonsy.silva@untrm.edu.pe)*

*[4]Centro Experimental Yanayacu, Dirección de Servicios Estratégicos Agrarios (DSEA), Instituto Nacional de Innovación Agraria (INIA), Carretera Jaén San Ignacio KM 23.7, Jaén 06801, Cajamarca, Peru*
*(e-mail: darwin.agroresearch@gmail.com)*

*[*]Corresponding authors*
*e-mail: jhon.zabaleta.epg@untrm.edu.pe; elgar.barboza@untrm.edu.pe*

(Received 9th Aug 2025; accepted 30th Jan 2026)

**Abstract.** Monitoring land use and land cover (LULC) changes is essential due to its close relationship with ecological processes, land-use planning, and environmental sustainability. In the Jucusbamba River sub-basin (Amazonas, Peru), knowledge of spatial transitions and cover change dynamics remains limited. This study analyzed LULC changes from 1992 to 2022 using Landsat and Sentinel satellite imagery classified with the Random Forest algorithm on the Google Earth Engine (GEE) platform. Additionally, future scenarios for 2037 and 2052 were simulated using the MOLUSCE plugin along with Artificial Neural Networks (ANN). Five main land cover classes were the followings: urban areas, pasture and cropland mosaics, forests, grasslands, and secondary shrub/herbaceous vegetation. Between 1992 and 2022, pasture/cropland mosaics increased by 24.36% and urban areas by 0.76%, while forests and secondary vegetation decreased by 8.89% and 16.25%, respectively. Projections to 2052 indicate further expansion of agricultural (4.74%) and urban (0.07%) land use, along with additional losses in forest cover (-1.47%) and secondary vegetation (-3.35%). The classification achieved an overall accuracy of 89.8% and a Kappa


http://www.aloki.hu ● ISSN 1589 1623 (Print) ● ISSN 1785 0037 (Online)
DOI: http://dx.doi.org/10.15666/aeer/2403_49654993
© 2026, ALÖKI Kft., Budapest, Hungary

coefficient of 0.86. These findings provide a robust foundation for evidence-based decision-making in land management, ecological zoning, and natural resource conservation within the Andean-Amazonian region.
**Keywords:** *spatial modeling, deforestation dynamics, remote sensing classification, sustainable landscape planning, Andean-Amazon transition zone*

## Introduction

Land use and land cover (LULC) changes are among the main drivers of environmental transformation on a global scale, with significant implications for climate, biodiversity, ecosystem services, and the socio-economic sustainability of territories (Admasu et al., 2023; Kah et al., 2025; Zafar et al., 2025). These processes—driven primarily by agricultural expansion, urbanization, industrialization, and population growth (Tiye et al., 2025), —generate widespread patterns of deforestation, landscape fragmentation, and forest degradation (World Bank, 2022). Collectively, they are responsible for approximately 10–15% of global greenhouse gas emissions (Rahaman et al., 2022; Schwamback et al., 2024).

According to estimates by the Food and Agriculture Organization of the United Nations (FAO), approximately 178 million hectares of forest cover were lost worldwide between 1990 and 2020, with tropical regions being the most severely affected (Abbas et al., 2020; Abhilash, 2021). These territorial transformations trigger cascading impacts, including soil erosion, loss of critical habitats, and disruptions to hydrological cycles, thereby compromising key ecosystem functions such as carbon sequestration, water regulation, and biodiversity conservation (Anteneh, 2022; Shiferaw et al., 2023). In tropical mountain regions, these impacts tend to be intensified due to high environmental heterogeneity and the complex interactions between biophysical and anthropogenic drivers (Armenteras et al., 2019; Pizarro et al., 2022)

In response to this growing challenge, systematic LULC monitoring has become a scientific and territorial management priority (Afuye et al., 2024; Alegbeleye et al., 2024). Remote sensing (RS), combined with cloud-computing platforms such as Google Earth Engine (GEE) and machine learning (ML) algorithms, has enabled substantial advances in thematic mapping, historical change detection, and the simulation of future scenarios with high spatial and temporal accuracy (Gorelick et al., 2017; Srivastava and Chinnasamy, 2021; Kassaye et al., 2024). In particular, classification models based on Random Forest (RF) have demonstrated outstanding performance in analyzing large multitemporal datasets, while artificial neural networks (ANN) have emerged as robust tools for modeling complex nonlinear relationships and projecting landscape change trajectories (Breiman, 2001; Talukdar et al., 2020; Parracciani et al., 2024).

Although these methodological approaches have been widely applied and validated across diverse geographic contexts (Yin et al., 2023; Wen et al., 2024), their implementation remains limited in ecologically fragile areas such as the Peruvian Andean–Amazon region. In this region, most existing studies have focused on localized deforestation assessments or short-term multitemporal analyses, generally conducted at broad regional scales, without simultaneously integrating explicit landscape transition analysis and prospective simulation of future scenarios at the watershed scale (Rodríguez-Echeverry et al., 2018; Agudelo-Hz et al., 2023). This limitation constrains a comprehensive understanding of spatial land use change trajectories and reduces the capacity to anticipate their environmental and territorial implications in highly complex socio-ecological systems.


http://www.aloki.hu ● ISSN 1589 1623 (Print) ● ISSN 1785 0037 (Online)
DOI: http://dx.doi.org/10.15666/aeer/2403_49654993
© 2026, ALÖKI Kft., Budapest, Hungary

Within this context, the Jucusbamba River Basin, located in northeastern Peru (Amazonas region), represents a strategically important ecological system characterized by high biological diversity, rugged topography, and increasing anthropogenic pressure associated with agricultural expansion and changes in rural settlement dynamics. Despite its environmental and productive relevance, the basin exhibits a marked lack of continuous historical spatial information and predictive modeling of its territorial dynamics, which has hindered the formulation of evidence-based land-use planning and management strategies.

To address this knowledge gap, the present study proposes a distinctive approach compared to previous research conducted in the Andean Amazon by integrating multidecadal historical cartography (1992–2022), explicit spatial analysis of landscape transitions, and the simulation of future scenarios (2037 and 2052) within a single, reproducible methodological framework. Unlike studies that apply land use change models without jointly incorporating biophysical and anthropogenic variables, this work integrates topographic, accessibility, and human pressure factors as conditioning variables, enabling a more realistic representation of spatial landscape transformation trajectories at the watershed scale (Wang et al., 2022; Agudelo-Hz et al., 2023). The combined application of Google Earth Engine and artificial neural networks in the Jucusbamba River Basin therefore constitutes a novel methodological contribution for the anticipatory assessment of deforestation and land use change processes in tropical mountain regions.

In line with this methodological and scientific contribution, the objectives of this study are to: (i) generate multitemporal maps of land use and land cover changes in the Jucusbamba River Basin for the period 1992–2022 using Landsat and Sentinel imagery processed on the Google Earth Engine platform through the Random Forest algorithm; (ii) analyze spatial dynamics and landscape transitions based on the generated cartography, identifying the main conversion patterns between natural covers and anthropogenic land uses; and (iii) simulate future land use and land cover scenarios for the years 2037 and 2052, based on identified historical trends, using artificial neural networks implemented in the MOLUSCE plugin and incorporating biophysical and anthropogenic variables as conditioning factors.

This study proposes a replicable methodology that combines cloud-based geospatial processing with artificial intelligence–based modeling techniques to generate robust scientific evidence supporting land-use planning, sustainable natural resource management, and environmental conservation in ecologically vulnerable regions such as the Peruvian Andean Amazon, particularly within the Jucusbamba River Basin.

## Materials and methods

### *Study area*

The Jucusbamba micro-watershed is located in the northeastern region of Peru, specifically within the province of Luya, Amazonas department. Geographically, it lies between UTM coordinates 176,703.42 m E and 9,329,116.67 m S, within zone 18S of the WGS84 reference system. The watershed covers an approximate area of 191.67 km² and includes the districts of San Cristóbal, Lámud, Luya, Trita, Inguilpata, and Lonya Chico (*Figure 1*).

It is bordered to the east by the province of Chachapoyas, to the west by Chota (Cajamarca), to the south by Celendín, and to the north by Bongará. The area features


http://www.aloki.hu ● ISSN 1589 1623 (Print) ● ISSN 1785 0037 (Online)
DOI: http://dx.doi.org/10.15666/aeer/2403_49654993
© 2026, ALÖKI Kft., Budapest, Hungary

predominantly mountainous terrain, with elevations ranging from 2,000 to 3,000 meters above sea level, characteristic of the northeastern Andes. The climate corresponds to a temperate humid montane type, with average annual temperatures between 12 °C and 18 °C and precipitation exceeding 1,000 mm per year, mainly concentrated between October and April.

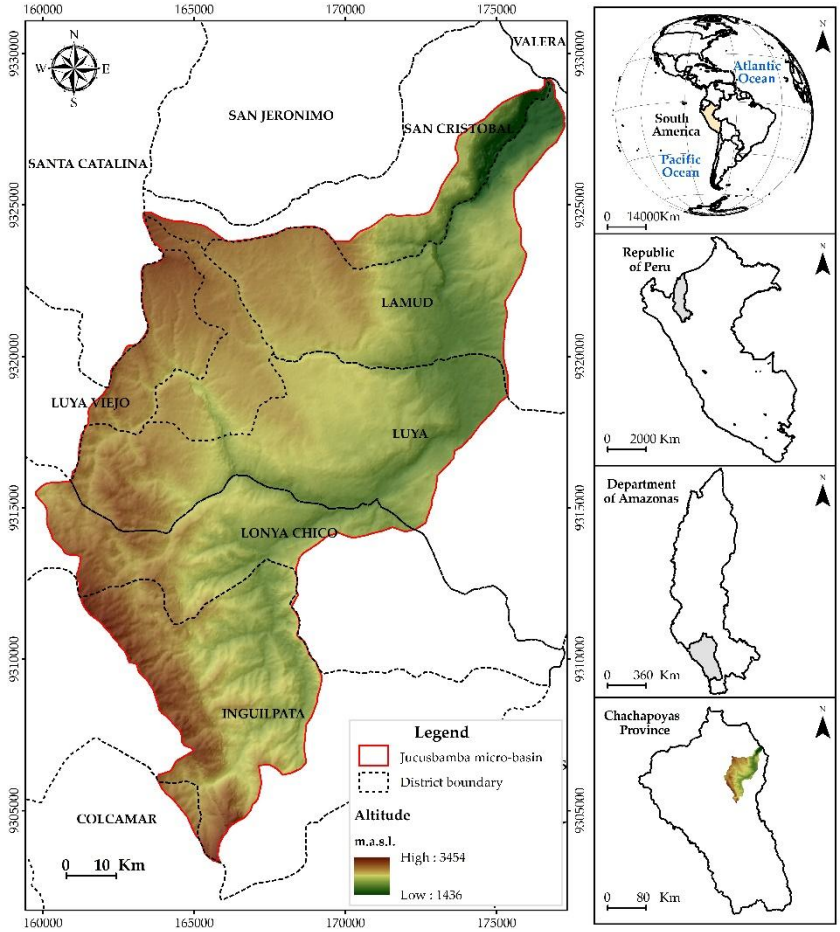


***Figure 1.*** *Area of influence of the Jucusbamba micro-watershed*

From an ecological standpoint, the micro-watershed is part of the humid montane Andean ecosystems. According to the ecological classification of the Peruvian Ministry of the Environment (MINAM, 2016a), the primary vegetation cover includes upper montane forest (Bm-al), montane forest (Bm-mo), jalca formations (Jal), and non-Amazonian forest areas (Ano-ba). Additionally, studies conducted by the Peruvian Amazon Research Institute (IIAP) and the Regional Government of Amazonas (IIAP & GOREA, 2016) report the presence of humid shrublands and remnants of high-elevation cloud forests, which play a critical role in water regulation and biodiversity conservation.

From a sociocultural perspective, the micro-watershed harbors significant archaeological and touristic heritage. Among its main attractions are the Karajía Sarcophagi and the Quiocta Caverns, located at approximately 2,700 meters above sea level. At its southern boundary lies the Huaylla Belén – Colcamar Private Conservation Area (ACP), a site dedicated to the protection of natural resources and the promotion of community-based ecotourism.


http://www.aloki.hu ● ISSN 1589 1623 (Print) ● ISSN 1785 0037 (Online)
DOI: http://dx.doi.org/10.15666/aeer/2403_49654993
© 2026, ALÖKI Kft., Budapest, Hungary

The Jucusbamba basin constitutes a strategic setting for analyzing land use and land cover changes due to its high ecological sensitivity, the dynamism of its agriculture- and livestock-based productive matrix, and its increasing exposure to anthropogenic transformation processes and environmental degradation.

### *Methodological workflow*

This study employed a quantitative and geospatial approach to analyze and predict LULC changes in the Jucusbamba micro-watershed (Amazonas, Peru) over the period 1992–2052. To achieve this, the methodology integrated remote sensing techniques, spectral analysis, supervised classification, and predictive modeling using artificial intelligence algorithms.

The methodological process was structured into four main stages:
(i) acquisition and preprocessing of satellite imagery,
(ii) spectral processing and analysis,
(iii) change detection and generation of transition matrices, and
(iv) predictive modeling using the MOLUSCE plugin (*Figure 2*).

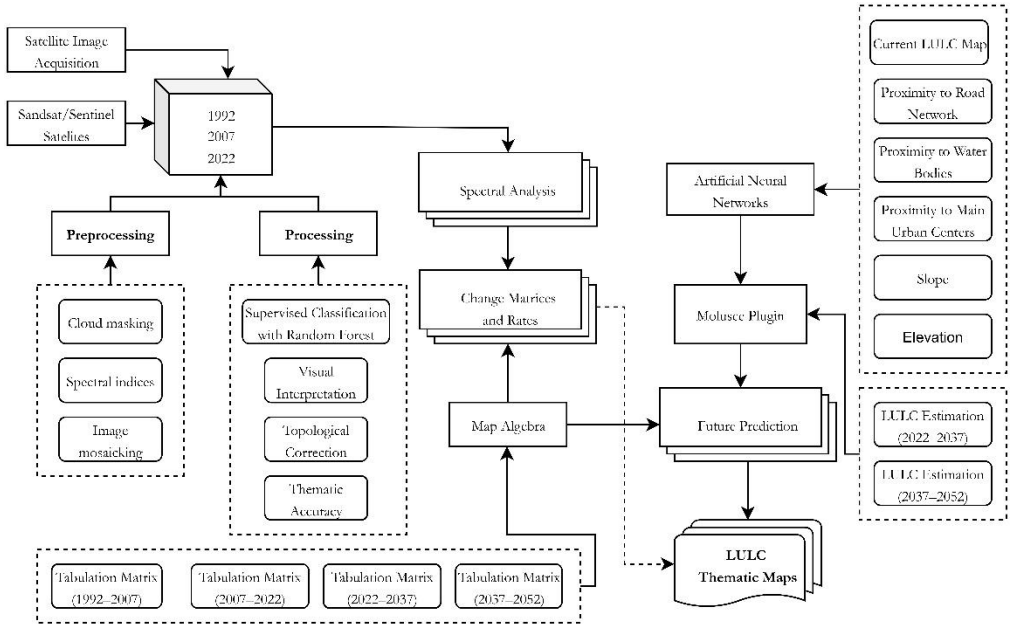


***Figure 2.*** *Methodological workflow for predicting land use and land cover (LULC) changes in the Jucusbamba micro-watershed, Amazonas, Peru*

The methodological framework of this study was structured into four main stages, designed to integrate the analysis of historical and future changes in land use and land cover within the Jucusbamba River Basin. In the first stage, Landsat and Sentinel satellite imagery corresponding to the years 1992, 2007, and 2022 was acquired and preprocessed using standard procedures, including atmospheric correction, cloud filtering, and the generation of multitemporal composites.

In the second stage, the processed imagery was classified using the Random Forest algorithm to produce thematic land use and land cover maps, which were subsequently validated with field data and refined through visual interpretation and topological correction.


http://www.aloki.hu ● ISSN 1589 1623 (Print) ● ISSN 1785 0037 (Online)
DOI: http://dx.doi.org/10.15666/aeer/2403_49654993
© 2026, ALÖKI Kft., Budapest, Hungary

Based on this cartography, the third stage involved the analysis of spatial changes and landscape transitions across the different study periods, employing change matrices and rates of variation to identify the main conversion dynamics between natural land covers and anthropogenic uses.

Finally, in the fourth stage, future land use and land cover change scenarios for the years 2037 and 2052 were simulated using a cellular automata and artificial neural network model, incorporating environmental and accessibility variables as conditioning factors. This methodological framework enabled a coherent linkage between historical cartography, change analysis, and future scenario prediction within a reproducible and comprehensible approach.

## *Land use and land cover change*

### *Acquisition and preprocessing of satellite images*

Geospatial data processing and analysis were conducted using a combination of open-source and commercial software platforms, including QGIS, Google Earth Engine (GEE), ArcGIS, and Google Earth Pro. These tools were used for image preprocessing, thematic classification, spatial analysis, and cartographic representation.

Field data collection was carried out using a Garmin Montana 650 handheld GPS receiver, which allowed for precise georeferencing of ground control and verification points. As cartographic reference, official datasets were used, including 1:100,000-scale national maps produced by the National Geographic Institute (IGN), vector layers of political-administrative divisions generated by the National Institute of Statistics and Informatics (INEI), as well as the national road network provided by the Ministry of Transport and Communications (MTC, 2022).

To characterize the elevation of the study area, digital elevation models (DEMs) were incorporated—specifically the ALOS PALSAR product with a spatial resolution of 12.5 meters (Logan et al., 2014), developed by the Japan Aerospace Exploration Agency (JAXA), complemented by SRTM data with a 30-meter resolution. The combination of these sources ensured accurate terrain representation and improved the precision of spatial analyses.

Multitemporal satellite imagery was acquired for three reference periods using Landsat 5 TM (1989–1992), Landsat 7 ETM+ (2004–2007), and Sentinel-2A (2019–2022) sensors through the Google Earth Engine platform, accessing the USGS archive (Gorelick et al., 2017). Image selection was based on a cloud cover threshold below 40% and constrained to three-year temporal windows to ensure consistency across periods, following established methodological criteria (Riaño et al., 2003; Phan et a., 2020; van der Woude et al., 2024). The main characteristics, selection criteria, and spectral configurations of the satellite imagery used in this study are summarized in *Table 1*.

***Table 1.*** *Selection criteria and parameters of the satellite images used*

| Date Range | Satellite | Sensor | No. of Images Used | Cloud Cover Threshold | Spectral Bands Used |
|---|---|---|---|---|---|
| 1989-01-01 to 1992-05-31 | Landsat 5 TM | TM | 7 | < 40% | 1, 2, 3, 4, 5, 6, 7 |
| 2004-01-01 to 2007-05-31 | Landsat 7 ETM+ | ETM+ | 8 | | |
| 2019-01-01 to 2022-05-31 | Sentinel-2A | MSI | 27 | < 40% | 1–12 (including 8A, 10, 11) |


http://www.aloki.hu ● ISSN 1589 1623 (Print) ● ISSN 1785 0037 (Online)
DOI: http://dx.doi.org/10.15666/aeer/2403_49654993
© 2026, ALÖKI Kft., Budapest, Hungary

Image preprocessing on the GEE platform followed a three-step workflow: cloud and shadow masking, calculation of spectral indices to enhance land cover discrimination, and generation of multitemporal mosaics representing average conditions for each period (Zhang et al., 2024; Tian et al., 2025; Yasin et al., 2025). A detailed list of spectral indices is provided in the Supplementary Material (*Table A1*).

Finally, multitemporal mosaics were generated by integrating imagery acquired across multiple dates within each analysis period, producing representative composites that capture the average environmental conditions of each time interval and reduce the influence of short-term variability (Yasin et al., 2025).

In addition to spectral information, auxiliary topographic variables derived from digital elevation models—including elevation, slope, and aspect—were incorporated into the classification process. These variables provide essential information on terrain constraints and were used to improve class separability and overall model performance, particularly in mountainous landscapes such as the Jucusbamba River Basin (Jin et al., 2018; Ganjirad and Bagheri, 2024).

*Land use and land cover classification*

The thematic classification of land use and land cover was carried out using a hierarchical methodology adapted from the CORINE Land Cover system and contextualized for Peruvian territory according to guidelines established by the MINAM (2015), This approach was reinforced through field observations and direct on-site validation using a total of 196 georeferenced control points collected via GPS receivers, which enabled verification and adjustment of classification accuracy.

The classification system was structured into three hierarchical levels, allowing for a progressive representation of thematic detail. At the first level, five major land cover categories were defined (*Table 2*): urbanized areas (ZU), pasture and cropland mosaics (PC), forest formations (BO), high Andean grasslands and shrublands (PH), and secondary shrub/herbaceous vegetation (AH). This typology was based on ecological, structural, and functional criteria, facilitating both the interpretation of spatial patterns and the temporal comparison of landscape changes.

***Table 2.*** *Hierarchical classification system for land use and land cover*

| Level | Level II | Level III | LULC Code |
|---|---|---|---|
| Artificial Areas | 1.1. Urbanized Areas | 1.1.1. Continuous urban fabric<br>1.1.2. Discontinuous urban fabric | ZU |
| Agricultural Areas | 2.4. Heterogeneous agricultural areas | 2.4.2. Pasture and cropland mosaic | PC |
| Forests and predominantly natural areas | 3.1. Forests | 3.1.1. Dense low forest<br>3.1.2. Open low forest<br>3.1.3. Dense high forest<br>3.1.4. Open high forest | BO |
| | 3 3.3. Herbaceous and/or shrub vegetation areas | 3.3.1. Grassland/Pajonal | PH |
| | | 3.3.4. Shrub/herbaceous vegetation<br>3.3.7. Disturbed shrub–grassland area | AH |

*Supervised classification using Random Forest*

For the supervised classification of land use and land cover, the RF algorithm was selected due to its proven effectiveness in processing satellite imagery for the detection


http://www.aloki.hu ● ISSN 1589 1623 (Print) ● ISSN 1785 0037 (Online)
DOI: http://dx.doi.org/10.15666/aeer/2403_49654993
© 2026, ALÖKI Kft., Budapest, Hungary

and differentiation of land cover types (Rodriguez-Galiano et al., 2012; Xia et al., 2017; Moraes et al., 2024). This machine learning approach is based on the construction of multiple decision trees, allowing it to handle noisy data, manage highly correlated variables, and achieve higher classification accuracy compared to traditional parametric classifiers (Gislason et al., 2006; Liu et al., 2025).

The model configuration included the generation of 10 decision trees, which were trained using spectral signatures derived from field sampling points. This training strategy ensured a robust and representative characterization of the thematic classes considered in the classification process, improving the model's stability and predictive performance.

*Visual validation and interpretation*

To verify the consistency of the classification results and correct potential classification errors, a detailed visual interpretation of the satellite imagery was conducted. This step followed the methodological protocol established by the FAO (1996), later updated by Osorio et al. (2015).

The procedure involved the manual review of the most evident inconsistencies generated by the automated classifier, comparing the thematic assignments with the actual visual appearance of land cover in the satellite images. This visual validation process improved the final accuracy of the generated maps, ensuring a stronger correspondence between the classified land cover categories and the observed ground conditions.

*Topological correction and vector conversion*

Once the classification stage was completed, the raster data were converted into vector format to facilitate cartographic representation and subsequent spatial analysis. During this conversion process, rigorous topological rules were applied to eliminate typical digitization errors, such as overlapping polygons, gaps, or invalid geometries.

In addition, a threshold of 0.5 hectares was defined as the Minimum Mappable Unit (MMU), in accordance with the methodological guidelines proposed by Vargas (1992). This criterion allowed the exclusion of spurious or insignificant polygons that did not represent meaningful analytical units. However, exceptions were made for specific classes such as urban areas, which often occupy small surfaces but hold high thematic relevance. These were retained in the final product in order to preserve the classification's consistency and level of detail (*Figure 3*).

***Thematic accuracy assessment***

To assess the thematic accuracy of the LULC classification, the statistical formula proposed by Cochran (1977), was applied. A total of 302 verification sites were used, stratified according to observed land cover units. Fieldwork further supported this validation, aligning classified data with direct observations, following the methodological recommendations of Rojas et al. (2019).

A confusion matrix (*Table A2*) was then generated, based on the structure described by Chuvieco (2007) and adopted by Peru's (MINAM, 2015), to evaluate the agreement between satellite image classifications and actual ground reference data (Chuvieco, 2020). n this matrix, rows represent the classes generated by the classification algorithm, while columns indicate the reference classes used for validation. The main diagonal reflects the number of exact matches, while off-diagonal values reveal commission errors (incorrect class assignment) and omission errors (classes not detected by the model).


http://www.aloki.hu ● ISSN 1589 1623 (Print) ● ISSN 1785 0037 (Online)
DOI: http://dx.doi.org/10.15666/aeer/2403_49654993
© 2026, ALÖKI Kft., Budapest, Hungary

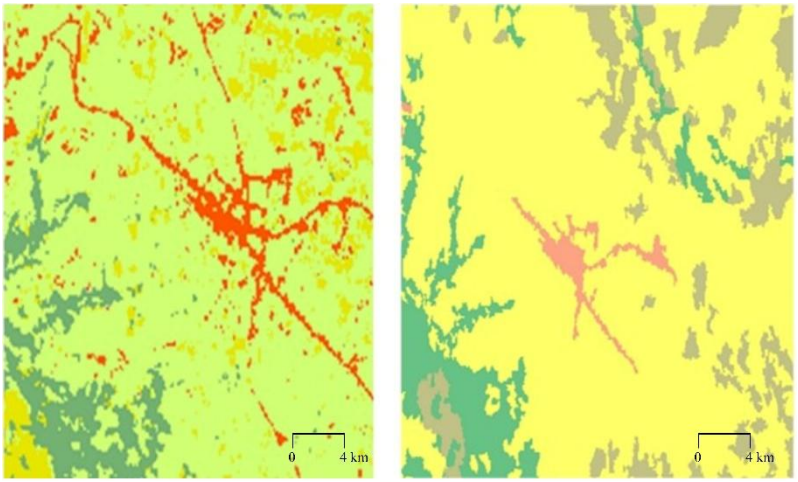


***Figure 3.*** *Comparison between supervised classification before and after applying topological correction*

From the confusion matrix, overall accuracy was calculated as the ratio between the number of correctly classified observations and the total number of observations. Additionally, the Kappa coefficient (κ) was computed using *Eq.1*, which quantifies agreement between classification and reference data adjusted for chance agreement (Rojas et al., 2019).

$$k = \frac{m\sum_{n=1}^{r} a_{nn} - \sum_{n=n}^{r} a_{n+}a_{+n}}{m^2 - \sum_{n=n}^{r} a_{n+}a_{+n}} \quad \text{(Eq.1)}$$

where:

- r is the number of rows in the confusion matrix (*Table A1*),
- $a_{nn}$ is the number of correctly classified observations for class n,
- $a_n$+$a_{+n}$ are the marginal totals for row and column n,
- m is the total number of observations.

These accuracy metrics provide a robust evaluation of the classification performance, indicating a high level of agreement between the classified maps and independent reference data. The achieved overall accuracy and Kappa coefficient exceed commonly accepted thresholds in land use and land cover studies, supporting the reliability of the generated cartographic products as inputs for subsequent change detection and predictive modeling

### *Spatiotemporal analysis of change: Rates, matrices, and transitions*

The spatial dynamics of LULC change were analyzed using map algebra to estimate differences in land cover area for each comparative period. For this purpose, the annual rate of change was calculated using the FAO (1996) formula:

$$s = \left(\frac{S_2}{S_1}\right)^{1/t_2 - t_1} - 1 \quad \text{(Eq.2)}$$

where $a_1$ and $a_2$ represent the land cover areas in years $t_1$ and $t_2$, respectively. A negative *s* value indicates cover loss, while a positive value denotes gain.


http://www.aloki.hu ● ISSN 1589 1623 (Print) ● ISSN 1785 0037 (Online)
DOI: http://dx.doi.org/10.15666/aeer/2403_49654993
© 2026, ALÖKI Kft., Budapest, Hungary

To examine category-level transitions, cross-tabulation (or change) matrices were created (*Table A3*), identifying losses ($L_i$), gains ($G_j$), net change ($C_n$), total change ($C_t$), and swaps (Int) between classes, following the framework proposed by Pontius et al. (2004). The main diagonal represents unchanged areas, while off-diagonal cells capture land cover conversions from one class to another.

### *Future LULC change prediction (2022–2052)*

Future scenarios of land use and land cover (LULC) change were simulated using the MOLUSCE plugin (Modules for Land Use Change Simulation), integrated into the QGIS software environment. This tool enables the modeling of landscape dynamics based on historical land cover transitions between pairs of reference maps, using machine learning–based predictive algorithms.

To calibrate and project the model, three sequential temporal pairs of land cover maps were employed: (i) 1992–2007 to simulate the 2022 scenario, (ii) 2007–2022 to estimate conditions for 2037, and (iii) 2022–2037 to project land cover patterns for 2052. This stepwise approach allowed the model to incorporate recent spatial and temporal trends into future scenario estimation, improving the internal consistency and plausibility of long-term projections.

The predictive model was driven by a set of environmental and accessibility variables selected for their documented influence on land transformation processes in mountainous Andean–Amazonian landscapes (*Figure 4*). These variables included elevation and slope, which impose biophysical constraints on agricultural suitability, settlement patterns, and infrastructure development, particularly in steep terrain (El-Tantawi et al., 2019; Wang et al., 2022), as well as distance to rivers, roads, and population centers, which represent gradients of accessibility and anthropogenic pressure that facilitate land-use intensification and agricultural expansion (Abbas et al., 2021; Anteneh, 2022; Diep et al., 2025).

All predictor layers were processed in raster format and normalized prior to integration into the CA–ANN model, enabling the identification of areas with a higher probability of land cover transition based on the interaction between biophysical constraints and accessibility factors. In the Jucusbamba River Basin, this interaction plays a central role in shaping both historical and projected land cover trajectories, justifying the inclusion of these variables as conditioning factors in the predictive modeling framework.

The reliability of future LULC projections was evaluated by assessing the model's capacity to reproduce observed historical transitions. Specifically, the comparison between the simulated and observed 2022 land cover maps using the Kappa index provided an indirect but robust validation of the model's predictive performance, supporting its application for scenario-based analysis rather than deterministic forecasting.

Finally, land cover transitions were simulated using a Cellular Automata–Artificial Neural Network (CA–ANN) modeling approach. The accuracy of the simulated scenarios was assessed through the Kappa index by comparing the projected land use map with the observed land cover for 2022. The model was configured with 100 iterations, a 1×1 pixel neighborhood, a learning rate of 0.001, 12 hidden layers, and a momentum factor of 0.00.


http://www.aloki.hu ● ISSN 1589 1623 (Print) ● ISSN 1785 0037 (Online)
DOI: http://dx.doi.org/10.15666/aeer/2403_49654993
© 2026, ALÖKI Kft., Budapest, Hungary

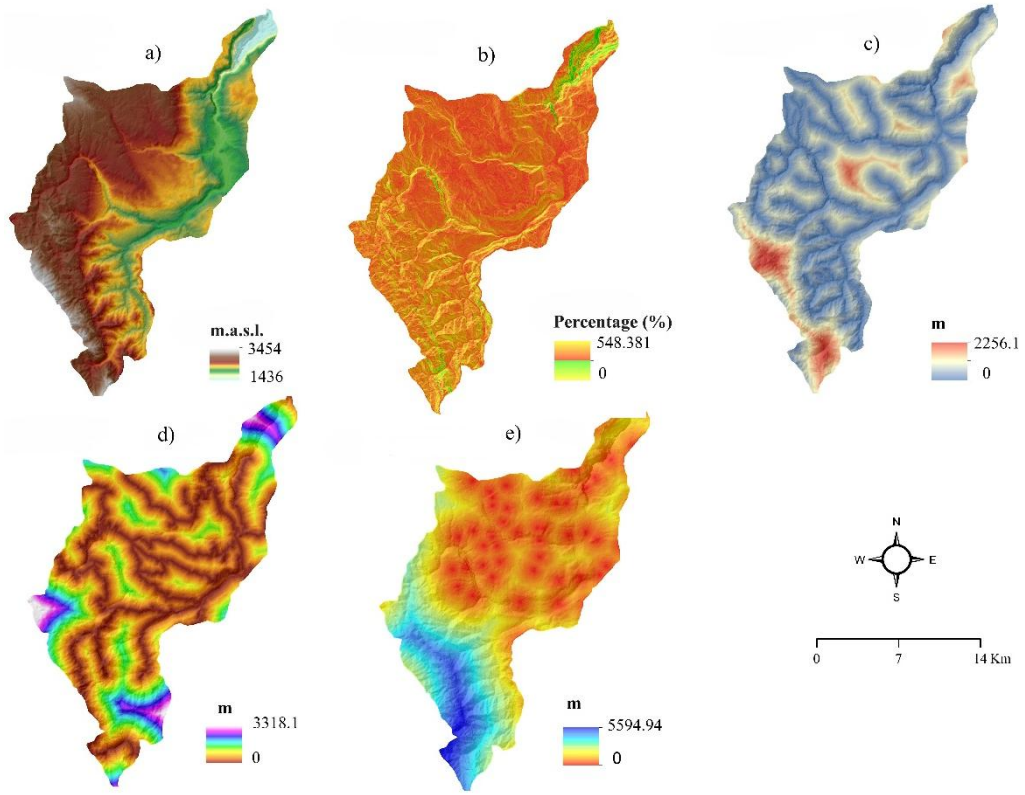


***Figure 4.*** *Environmental and accessibility predictor variables used for land use and land cover (LULC) change modeling in the Jucusbamba River Basin. The figure shows the spatial distribution of key conditioning variables: (a) elevation (m a.s.l.), (b) slope (%), (c) distance to rivers (m), (d) distance to roads (m), and (e) distance to population centers (m), which jointly represent the biophysical constraints and anthropogenic accessibility gradients influencing historical and projected land cover transitions*

## *Forest loss concentration analysis*

To evaluate the spatial concentration of forest cover loss, land use and land cover maps were compared across four time intervals: 1992–2007, 2007–2022, 2022–2037, and 2037–2052. This multitemporal analysis allowed the identification of both historical and projected deforestation trends, as well as the spatial patterns associated with these processes.

To pinpoint areas with the highest intensity of forest cover loss, the Kernel Density Estimation method was applied. This technique generates a continuous surface reflecting the spatial concentration of change events, allowing for the identification of hotspots where deforestation is most frequent or severe. The approach integrates both anthropogenic and natural drivers.

This methodology was implemented in accordance with the technical guidelines of the Peruvian (MINAM, 2016b), ensuring methodological consistency with national forest monitoring standards. The outputs from the spatial density analysis represent a critical tool for informing conservation strategies, territorial management, and environmental planning in areas experiencing high ecological pressure.


http://www.aloki.hu ● ISSN 1589 1623 (Print) ● ISSN 1785 0037 (Online)
DOI: http://dx.doi.org/10.15666/aeer/2403_49654993
© 2026, ALÖKI Kft., Budapest, Hungary

## Results

### *Historical land use and cover change (1992–2022)*

The dynamics of LULC in the Jucusbamba River micro-watershed were analyzed for the years 1992, 2007, and 2022 (*Figure 5*). During the first interval (1992–2007), a net loss of 605.15 hectares of forest cover was recorded, equivalent to 8% of the forest area in 1992, with an annual deforestation rate of approximately 40.34 hectares. In the subsequent period (2007–2022), this trend intensified, reaching a loss of 1,099.4 hectares—representing 15.8% of the 2007 forest area—with an annual rate of 73.29 hectares (see *Table A4*).

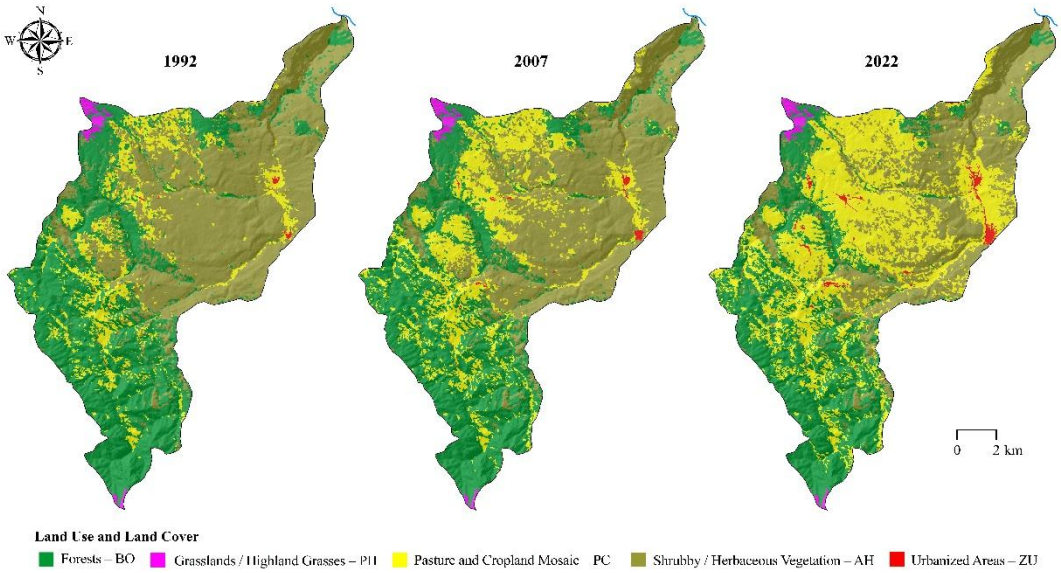


***Figure 5.*** *Land use and land cover in the Jucusbamba micro-watershed from 1992 to 2022*

This reduction in forest cover corresponded primarily to the expansion of pasture and cropland mosaics, which increased by 1,611.35 hectares between 1992 and 2007—a 70.96% increase relative to its initial extent—with an annual increase of 107.42 hectares. In the period 2007–2022, this land use class experienced even greater expansion, adding 3,057.78 hectares (a 78.76% increase over the 2007 figure), with an annual growth rate of 203.85 hectares.

To validate the 2022 LULC classification map, a correspondence analysis was conducted comparing thematic classes with field-based control points. *Table A5* presents the reference area distribution by thematic class, and *Table A6* summarizes the confusion matrix results. The analysis yielded an overall accuracy of 89.8% and a Kappa index of 0.86, demonstrating a high level of agreement between the classified data and the validation reference, thus supporting the reliability of the generated cartographic product.

The observed changes indicate a gradual transformation of the landscape, driven primarily by the expansion of anthropogenic activities. The comparison between the periods 1992–2007 and 2007–2022 (*Figure 6*) shows a sustained decline in forest cover, with respective losses of 3.16% and 5.74%, as well as a decrease in shrub and herbaceous vegetation, with reductions of 5.43% and 10.82%. Conversely, anthropogenic land covers increased, particularly pasture/cropland mosaics (up by 8.41% and 15.95%) and urban areas, which grew by 0.17% and 0.59% in the respective periods.


http://www.aloki.hu ● ISSN 1589 1623 (Print) ● ISSN 1785 0037 (Online)
DOI: http://dx.doi.org/10.15666/aeer/2403_49654993
© 2026, ALÖKI Kft., Budapest, Hungary

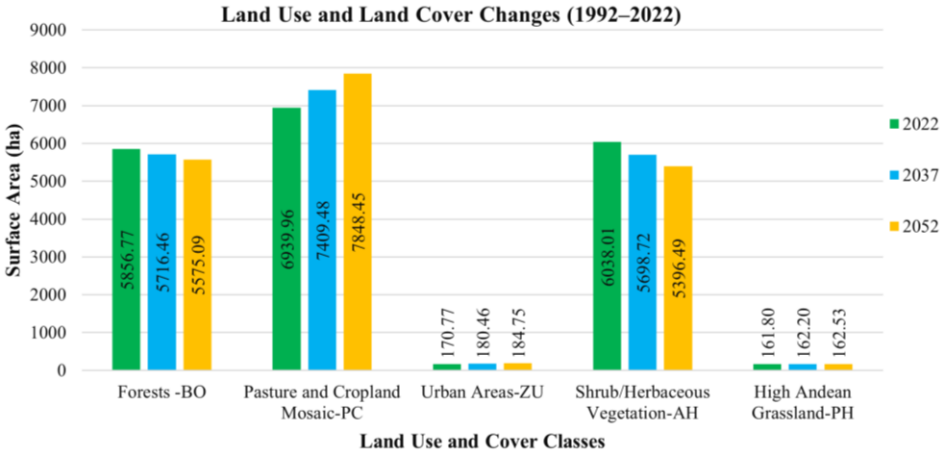


***Figure 6.*** *Land use and land cover changes from 1992 to 2022 in the Jucusbamba micro-watershed*

*Figure 7*, along with Tables A7 and A8, presents a detailed analysis of LULC changes in the Jucusbamba micro-watershed for the periods 1992–2007 and 2007–2022. The matrix-based structure used in the analysis allows for the identification of both stable land cover classes and those that underwent transformations. In the change matrix, the main diagonal represents land covers that remained unchanged during the analyzed interval, while the off-diagonal cells indicate transitions between classes. Each row and column corresponds to thematic classes from two distinct dates (date 1 and date 2, respectively), and their intersections reflect changes from one class to another.

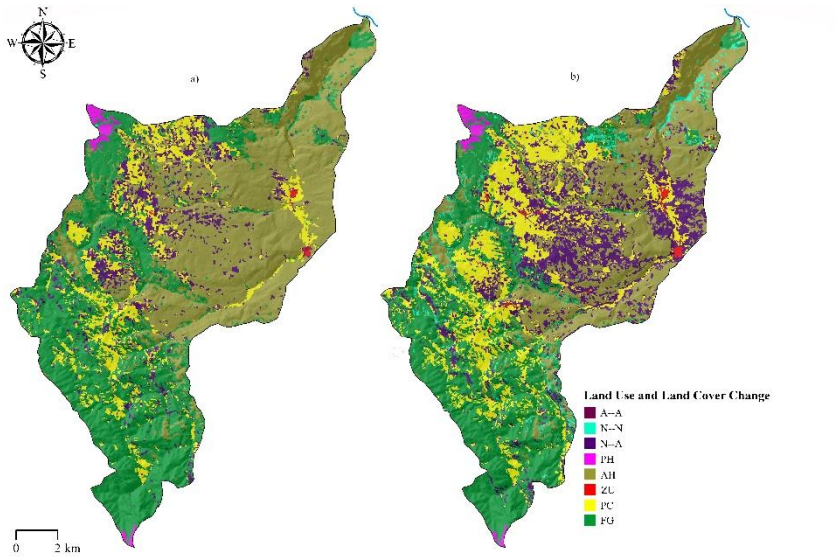


***Figure 7.*** *Land use and land cover (LULC) transition and persistence patterns in the Jucusbamba River micro-watershed during the periods 1992–2007 and 2007–2022. Panel (a) shows LULC transitions for the period 1992–2007, while panel (b) represents transitions observed between 2007 and 2022. Colors indicate land cover transition and persistence classes coded as A--A (anthropogenic to anthropogenic), N--N (natural to natural), N--A (natural to anthropogenic), PH (persistence of grasslands/high Andean grasslands), AH (persistence of shrub/herbaceous vegetation), ZU (urban persistence), PC (persistence of pasture–cropland mosaic), and FG (forest persistence*


http://www.aloki.hu ● ISSN 1589 1623 (Print) ● ISSN 1785 0037 (Online)
DOI: http://dx.doi.org/10.15666/aeer/2403_49654993
© 2026, ALÖKI Kft., Budapest, Hungary

The results show that the deforestation rate was significantly higher during the 2007–2022 period, reaching 1.14%, compared to 0.55% during 1992–2007. This vegetation loss dynamic is reflected in the systematic conversion of forest and shrub/herbaceous vegetation areas into pasture and cropland mosaics—an observed pattern consistent across both time intervals.

### *Forest loss concentration in the Jucusbamba micro-watershed (1992–2022)*

The spatial distribution of forest cover loss in the Jucusbamba micro-watershed is illustrated in *Figure 8* and categorized into five levels of concentration, as detailed in *Table A9*. For this analysis, two metrics were distinguished: Non-cumulative Area, representing the individual surface area of each concentration category, and Cumulative Area, indicating the progressive sum of those categories.

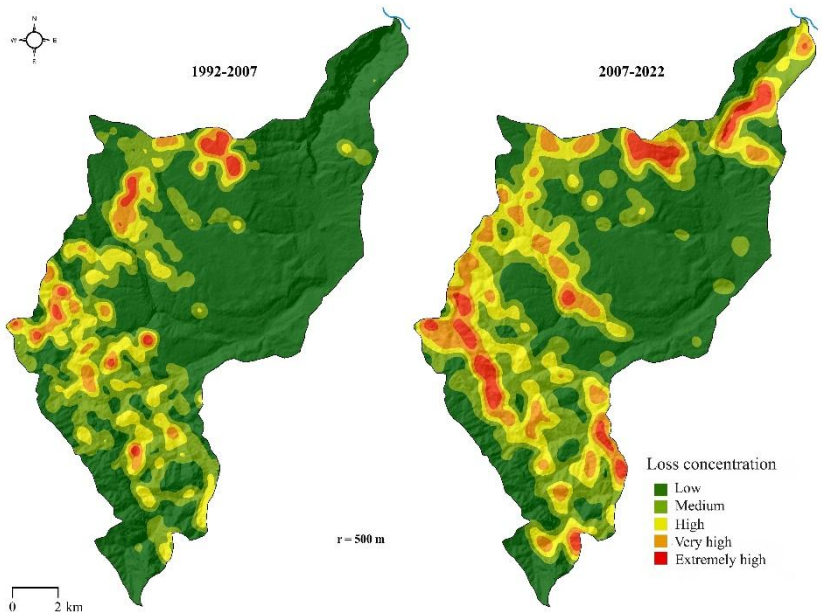


***Figure 8.*** *Forest loss concentration in the Jucusbamba micro-watershed during the 1992–2022 period*

During the 1992–2007 period, areas with low forest loss concentration accounted for 63.33% of the total, whereas in the 2007–2022 period, this category declined to 45.58%. These zones generally encompassed large expanses in comparison to areas classified as having extremely high concentration, which represented only 1.38% in the first period but increased to 3.93% in the second.

In cumulative terms, the extremely high concentration category remained below 4% of the total in both periods, indicating that while these zones are spatially limited, they exhibit intense localized deforestation. This pattern suggests a clear intensification of forest loss processes in specific landscape areas during the most recent interval.

### *Land use and land cover change maps in the Jucusbamba micro-watershed (2022–2052)*

The results of the spatial simulation of LULC for the years 2037 and 2052 in the Jucusbamba micro-watershed are shown in *Figure 9*. During the first projected period


http://www.aloki.hu ● ISSN 1589 1623 (Print) ● ISSN 1785 0037 (Online)
DOI: http://dx.doi.org/10.15666/aeer/2403_49654993
© 2026, ALÖKI Kft., Budapest, Hungary

(2022–2037), forest cover loss is estimated at 140.32 hectares, equivalent to 2.4% of the area recorded in 2022, with an average annual reduction rate of 9.35 ha/year. For the second period (2037–2052), the projected loss reaches 141.36 hectares, representing 2.5% of the 2022 forest cover, with a slightly higher deforestation rate of 9.42 ha/year (see *Table A10*).

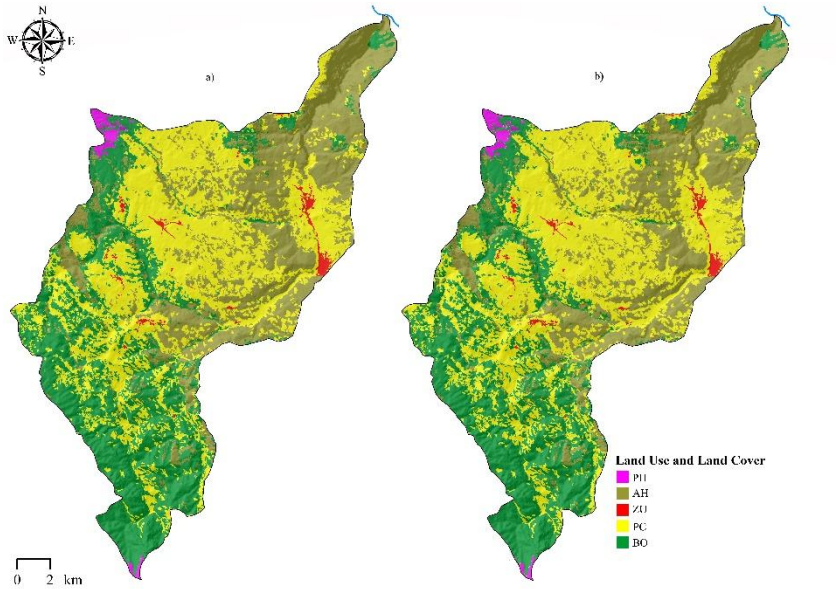


***Figure 9.*** *Projected land use and land cover (LULC) spatial patterns in the Jucusbamba River micro-watershed for the years 2037 and 2052. Panel (a) shows the projected LULC distribution for 2037, while panel (b) represents the projected scenario for 2052. Colors indicate land cover classes coded as PH (grasslands/high Andean grasslands), AH (shrub/herbaceous vegetation), ZU (urban areas), PC (pasture–cropland mosaic), and BO (forests)*

This reduction in forest area is reflected in the expansion of the pasture and cropland mosaic class. In the 2022–2037 scenario, this class increases by 469.52 hectares (equivalent to 6.77% of the 2022 area, with a growth rate of 31.30 ha/year). During the 2037–2052 period, this trend continues, with an additional increase of 438.97 hectares—5.92% of the 2037 area—at an annual rate of 29.23 ha/year. These projected changes are cartographically illustrated in *Figure 10*.

*Figure 11*, together with *Tables A10 and A11*, provides a detailed analysis of the projected LULC changes for the periods 2022–2037 and 2037–2052. The results suggest that the deforestation rate will be slightly higher in the second period (0.17%) compared to the first (0.16%), indicating a continued but marginally accelerated trend in forest cover loss.

Across both projection intervals, there is a consistent conversion of forest and shrub/herbaceous vegetation into pasture and cropland mosaics, highlighting an ongoing expansion of agricultural activity at the expense of natural vegetation.

Urban areas are also expected to continue expanding, with a projected growth rate of 0.37% for the 2022–2037 period, followed by an additional increase of 0.16% between 2037 and 2052. These values reflect a progressive trend of urban expansion, albeit with a slight deceleration in the longer-term projection.


http://www.aloki.hu ● ISSN 1589 1623 (Print) ● ISSN 1785 0037 (Online)
DOI: http://dx.doi.org/10.15666/aeer/2403_49654993
© 2026, ALÖKI Kft., Budapest, Hungary

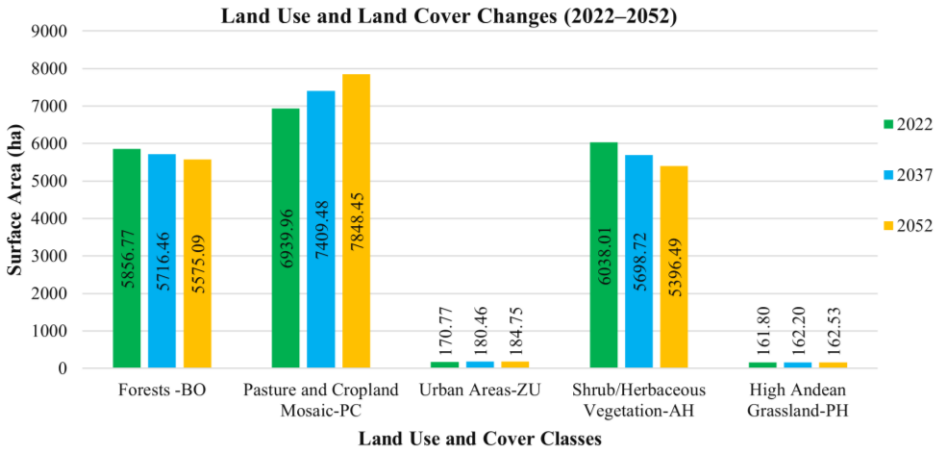


***Figure 10.*** *LULC changes from 1992 to 2022 in the Jucusbamba micro-watershed*

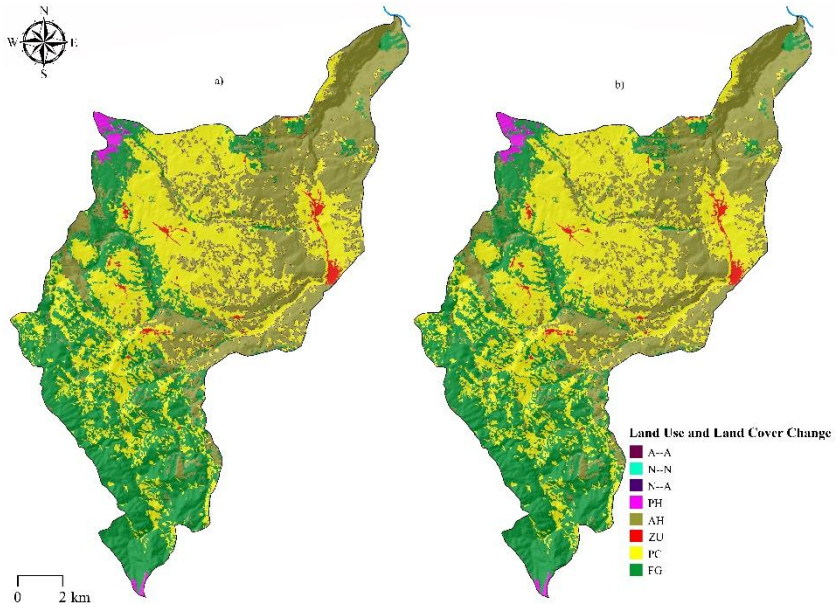


***Figure 11.*** *Projected land use and land cover (LULC) transition and persistence patterns in the Jucusbamba River micro-watershed for the periods 2022–2037 and 2037–2052. Panel (a) illustrates projected LULC transitions and persistence patterns for the period 2022–2037, while panel (b) represents the projected changes for 2037–2052. Colors denote transition and persistence classes coded as A→A (anthropogenic to anthropogenic), N→N (natural to natural), N→A (natural to anthropogenic), PH (persistence of grasslands/high Andean grasslands), AH (persistence of shrub/herbaceous vegetation), ZU (urban persistence), PC (persistence of pasture–cropland mosaic), and FG (forest persistence)*

## *Projected forest loss concentration in the Jucusbamba micro-watershed (2022–2052)*

The projected spatial distribution of forest cover loss is presented in *Figure 12* and classified into five concentration levels, as detailed in *Table A12*. This analysis distinguishes two metrics: the non-cumulative area, representing the individual surface area of each concentration class, and the cumulative area, reflecting the progressive sum of those classes.


http://www.aloki.hu ● ISSN 1589 1623 (Print) ● ISSN 1785 0037 (Online)
DOI: http://dx.doi.org/10.15666/aeer/2403_49654993
© 2026, ALÖKI Kft., Budapest, Hungary

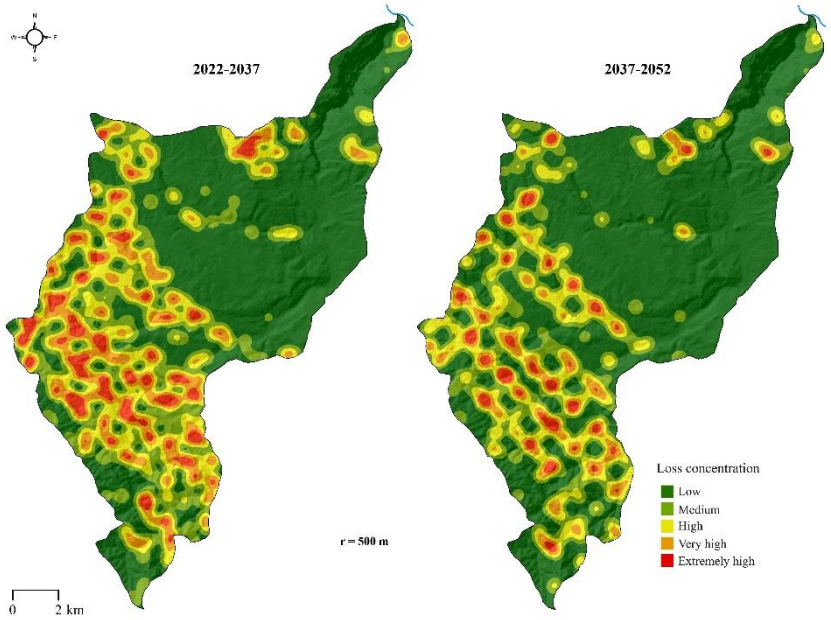


***Figure 12.*** *Projected forest loss concentration in the Jucusbamba micro-watershed during the 2022–2052 period*

In the 2022–2037 period, the low forest loss concentration class covered 50.06% of the total area, increasing to 61.35% during 2037–2052. This indicates that most of the projected deforestation will be dispersed across areas with relatively low intensity. In contrast, zones classified with extremely high loss concentration accounted for only 4.68% in the first period and decreased to 2.34% in the second.

In cumulative terms, areas with extremely high forest loss concentration remained below 4% across both intervals. This suggests that although deforestation in these zones is intense, their overall spatial extent remains limited. Such a characterization is useful for identifying priority areas for intervention and monitoring, particularly where deforestation processes are most concentrated.

## Discussion

The results of this study reveal an accelerated territorial transformation in the Jucusbamba micro-watershed, characterized by the progressive conversion of natural land covers (forests and secondary vegetation) into anthropogenic uses, primarily agriculture and urbanization. This trend is consistent with various regional and global studies that identify agricultural expansion, unplanned urban growth, and shifting cultivation as the primary drivers of land use change in mountain and Andean-Amazonian ecosystems (Admasu et al., 2023; Schwamback et al., 2024; Tiye et al., 2025).

During the analysis period (1992–2022), forest cover (BO) decreased by 8.89% and shrub/herbaceous vegetation (AH) by 16.25%, accompanied by a significant increase in the pasture and cropland mosaic (PC), which rose from 11.85% to 36.21%. These results are consistent with studies conducted in ecologically fragile areas, such as the Central Andes and Amazon transition basins, where the loss of natural vegetation is often replaced by heterogeneous agricultural systems. While these systems are economically


http://www.aloki.hu ● ISSN 1589 1623 (Print) ● ISSN 1785 0037 (Online)
DOI: http://dx.doi.org/10.15666/aeer/2403_49654993
© 2026, ALÖKI Kft., Budapest, Hungary

essential for rural livelihoods, they contribute to landscape fragmentation and reduced ecological connectivity (Shiferaw et al., 2023; Zafar et al., 2025).

The application of the RF algorithm for thematic classification proved to be both efficient and robust, as demonstrated by the high overall accuracy (89.8%) and Kappa coefficient (0.86)—both exceeding accepted thresholds for remote sensing studies focused on environmental monitoring (Gorelick et al., 2017; Moraes et al., 2024). This performance is consistent with findings Jin et al. (2018) and Parracciani et al. (2024), who emphasize the advantages of decision tree–based classifiers in mountainous regions with high spectral variability.

The land use transformation in the watershed is largely driven by socioeconomic and biophysical factors. Studies by Anteneh (2022) and Kassaye et al. (2024) highlight that proximity to roads, settlements, and specific topographic conditions (elevation, slope) influences the likelihood of land cover change. In this study, areas experiencing the highest anthropogenic pressure were located between 2400 and 3400 meters above sea level—an elevation range favorable for traditional crops and rural settlements—thus supporting the hypothesis of localized pressure on transitional ecosystems.

Kernel density analysis applied over the 1992–2022 period allowed the identification of critical deforestation hotspots with high spatial concentration. This aligns with findings by Rojas et al. (2019) for other watersheds in northern Peru. Such geospatial analysis is crucial for targeting intervention strategies, as it helps prioritize ecologically vulnerable areas and implement more efficient restoration, conservation, and environmental monitoring actions (MINAM, 2016a; Ganjirad and Bagheri, 2024).

The projected land use and land cover scenarios for the period 2022–2052 indicate that the dominant trends observed in recent decades are likely to persist in the Jucusbamba River micro-watershed. In particular, the continued expansion of agricultural and pasture mosaics emerges as the most probable trajectory, accompanied by a gradual but sustained reduction in forest and shrub/herbaceous vegetation. Similar trajectories have been reported for other Andean and tropical mountain systems, where land conversion processes tend to continue in the absence of effective regulatory interventions (Talukdar et al., 2020; Tiye et al., 2025). Although the projected deforestation rates are lower than those observed during the 2007–2022 period, their cumulative effect over time suggests a persistent pressure on remaining natural ecosystems.

From a practical and environmental perspective, these projected trajectories have important implications for ecosystem functioning within the watershed. The continued conversion of forests and secondary vegetation into agricultural land is likely to intensify landscape fragmentation and reduce ecological connectivity, processes that have been widely associated with biodiversity loss and reduced ecosystem resilience in mountain environments (Shiferaw et al., 2023; Liu et al., 2025). In addition, the progressive reduction of forest cover may affect key ecosystem services such as water regulation and soil protection, which are particularly critical in Andean basins characterized by steep topography and high hydrological sensitivity (Abhilash, 2021; World Bank, 2022).

In this context, the projected scenarios should be interpreted as plausible future trajectories rather than as deterministic predictions. This approach is consistent with previous studies that highlight the value of scenario-based analyses for supporting land use planning and environmental management under uncertainty (Talukdar et al., 2020; Srivastava and Chinnasamy, 2021). By identifying areas where forest loss and agricultural expansion are most likely to continue, the results provide a useful basis for


http://www.aloki.hu ● ISSN 1589 1623 (Print) ● ISSN 1785 0037 (Online)
DOI: http://dx.doi.org/10.15666/aeer/2403_49654993
© 2026, ALÖKI Kft., Budapest, Hungary

prioritizing monitoring efforts and guiding preventive conservation and territorial planning actions in the Jucusbamba River Basin.

Despite the strong performance of the classification and simulation models, the projected scenarios are subject to several sources of uncertainty. These include potential classification errors in the input maps, limitations associated with the spatial and temporal resolution of satellite imagery, and assumptions regarding the persistence of historical land use change patterns into the future. Additional uncertainty arises from the selection of conditioning variables and from socio-economic drivers that are not explicitly modeled, such as policy changes or market dynamics. Consequently, the future scenarios presented in this study should be interpreted as plausible trajectories of land use and land cover change rather than exact predictions.

This scenario is particularly concerning given that Peru's mountain ecosystems function as key regulators of water and reservoirs of biodiversity. Their degradation directly jeopardizes water security, agricultural productivity, and climate resilience for local communities (Abhilash, 2021; World Bank, 2022). Moreover, the ecological fragmentation observed in the land cover change maps compromises species mobility and reduces the ecosystem's capacity for natural regeneration (Shiferaw et al., 2023; Liu et al., 2025).

From a methodological standpoint, the integration of multitemporal Landsat and Sentinel datasets, the use of the GEE platform, and the implementation of artificial intelligence–based modeling confirm the effectiveness and replicability of this approach for long-term territorial monitoring (Srivastava and Chinnasamy, 2021; Yasin et al., 2025). This combination enables the generation of high-quality cartographic outputs that support territorial planning, natural resource management, and environmental policy at both local and regional levels.

Finally, this study underscores the urgent need to implement public policies focused on active ecological restoration, urban growth control, promotion of sustainable agroecological practices, and the strengthening of land management tools. Successful watershed restoration experiences in China, Ethiopia, and Colombia have shown that, with proper planning, it is possible to reverse soil degradation processes and recover essential ecosystem services (Admasu et al., 2023; Christmann et al., 2023).

## Conclusions

This study provides an integrated assessment of historical and projected land use and land cover (LULC) dynamics in the Jucusbamba River micro-watershed, covering the period from 1992 to 2052. By combining multitemporal satellite imagery, machine learning–based classification, and spatial simulation techniques, the research successfully identified and quantified the main trajectories of landscape transformation in a highly sensitive Andean–Amazonian environment.

The application of the Random Forest algorithm, validated through high overall accuracy (89.8%) and a strong Kappa coefficient (0.86), demonstrated its effectiveness for producing reliable LULC maps in complex mountainous terrains. The results reveal a sustained expansion of pasture and cropland mosaics and urban areas, accompanied by a progressive reduction of forest and shrub/herbaceous vegetation. These trends reflect increasing anthropogenic pressure on natural ecosystems and highlight a gradual loss of landscape connectivity and ecological functionality within the micro-watershed.


http://www.aloki.hu ● ISSN 1589 1623 (Print) ● ISSN 1785 0037 (Online)
DOI: http://dx.doi.org/10.15666/aeer/2403_49654993
© 2026, ALÖKI Kft., Budapest, Hungary

From a regional perspective, the observed and projected land cover changes have important implications for ecosystem services that are critical to local communities, including water regulation, soil protection, and biodiversity conservation. The identification of deforestation hotspots through Kernel density analysis provides actionable spatial information to support targeted conservation, restoration, and monitoring strategies, particularly in areas where forest loss is most concentrated.

The simulation of future scenarios using the CA–ANN model indicates that current land use trends are likely to persist in the absence of effective regulatory and planning interventions. Although projected deforestation rates are lower than those observed in recent decades, their cumulative impact suggests continued pressure on remaining forested areas, especially in mid-altitude zones characterized by favorable agroecological conditions and high accessibility.

Beyond its local relevance, the methodological framework developed in this study—integrating cloud-based geospatial processing, machine learning classification, and scenario-based modeling—offers a replicable and transferable approach for analyzing land use dynamics in other Andean and tropical mountain regions. As such, the results provide valuable scientific evidence to inform territorial planning, environmental policy, and sustainable land management strategies in regions facing similar challenges of land conversion and ecosystem degradation.

This study contributes to a clearer understanding of land use change processes in the Amazonas region of Peru and highlights the importance of adopting spatially informed land management approaches that reconcile agricultural development with the conservation of key ecosystem services.

**Data availability statement.** The data used to support the findings of this study are available from the corresponding author upon request.

**Acknowledgments.** The authors acknowledge and appreciate the support of the INDES-CES of the National University Toribio Rodríguez of Mendoza of Amazonas (UNTRM).

**Conflicts of interest.** The authors declare no conflict of interest.

## REFERENCES

[1] Abbas, S., Wong, M. S., Wu, J., Shahzad, N., Irteza, S. M. (2020): Approaches of satellite remote sensing for the assessment of above-ground biomass across tropical forests: Pan-tropical to national scales. – Remote Sensing 12(20): 1-38. doi:10.3390/rs12203351.

[2] Abbas, Z., Yang, G., Zhong, Y., Zhao, Y. (2021): Spatiotemporal change analysis and future scenario of LULC using the CA-ANN approach: A case study of the greater bay area, China. – Land 10(6): 584. doi:10.3390/land10060584.

[3] Abhilash, P. C. (2021): Restoring the unrestored: Strategies for restoring global land during the un decade on ecosystem restoration (un-der). – Land 10(2): 1-17. doi:10.3390/land10020201.

[4] Admasu, S., Yeshitela, K., Argaw, M. (2023): Impact of land use land cover changes on ecosystem service values in the Dire and Legedadi watersheds, central highlands of Ethiopia: Implication for landscape management decision making. – Heliyon 9(4): e15352. doi:10.1016/j.heliyon.2023.e15352.


http://www.aloki.hu ● ISSN 1589 1623 (Print) ● ISSN 1785 0037 (Online)
DOI: http://dx.doi.org/10.15666/aeer/2403_49654993
© 2026, ALÖKI Kft., Budapest, Hungary

[5] Afuye, G. A., Nduku, L., Kalumba, A. M., et al. (2024): Global trend assessment of land use and land cover changes: A systematic approach to future research development and planning. – Journal of King Saud University – Science 36(7). doi:10.1016/j.jksus.2024.103262.
[6] Agudelo-Hz, W. J., Castillo-Barrera, N. C., Uriel, M. G. (2023): Scenarios of land use and land cover change in the Colombian Amazon to evaluate alternative post-conflict pathways. – Scientific Reports 13(1): 1-14. doi:10.1038/s41598-023-29243-2.
[7] Alegbeleye, O. M., Rotimi, Y. O., Shomide, P., Oyediran, A., Ogundipe, O., Akintunde-Alo, A. (2024): Land use land cover (LULC) analysis in Nigeria: a systematic review of data, methods, and platforms with future prospects. – Bulletin of the National Research Centre 48(1): 127. doi:10.1186/s42269-024-01286-z.
[8] Anteneh, M. (2022): Analysis of Land Use/Land Cover Change and Its Implication on Natural Resources of the Dedo Watershed, Southwest Ethiopia. – Scientific World Journal 2022: 6471291. doi:10.1155/2022/6471291.
[9] Armenteras, D., Murcia, U., González, T. M., Barón, O. J., Arias, J. E. (2019): Scenarios of land use and land cover change for NW Amazonia: Impact on forest intactness. – Global Ecology and Conservation 17: e00567. doi:10.1016/j.gecco.2019.e00567.
[10] Breiman, L. (2001): Random Forests. – Machine Learning 45(1): 5-32. doi:10.1023/A:1010933404324.
[11] Christmann, T., Palomeque, X., Armenteras, D., et al. (2023): Disrupted montane forest recovery hinders biodiversity conservation in the tropical Andes. – Global Ecology and Biogeography 32(5): 793-808. doi:10.1111/geb.13666.
[12] Chuvieco, E. (2007): Teledetección ambiental: La observación de la Tierra desde el espacio. – Ariel Ciencia, Barcelona.
[13] Chuvieco, E. (2020): Fundamentals of satellite remote sensing: An environmental approach. – CRC press [Preprint], (March). doi.org/10.1201/9780429506482.
[14] Cochran, W. G. (1977): Sampling Techniques. – 3rd Edition. New York. doi:10.4236/ojs.2015.51004.
[15] Diep, N. T. H., Nguyen, N. T., Diem, P. K., Nguyen, C. T. (2025): Benefits and Trade-Offs from Land Use and Land Cover Changes Under Different Scenarios in the Coastal Delta of Vietnam. – Land 14(5): 1063. doi:10.3390/land14051063.
[16] El-Tantawi, A. M., Bao, A., Chang, C., Liu, Y. (2019): Monitoring and predicting land use/cover changes in the Aksu-Tarim River Basin, Xinjiang-China (1990–2030). – Environmental Monitoring and Assessment 191: 480. doi:10.1007/s10661-019-7478-0.
[17] Ganjirad, M., Bagheri, H. (2024): Google Earth Engine-based mapping of land use and land cover for weather forecast models using Landsat 8 imagery. – Ecological Informatics 80(January): 102498. doi:10.1016/j.ecoinf.2024.102498.
[18] Gislason, P. O., Benediktsson, J. A., Sveinsson, J. R. (2006): Random forests for land cover classification. – Pattern Recognition Letters 27(4): 294-300. doi:10.1016/j.patrec.2005.08.011.
[19] Gorelick, N., Hancher, M., Dixon, M., Ilyushchenko, S., Thau, D., Moore, R. (2017): Google Earth Engine: Planetary-scale geospatial analysis for everyone. – Remote Sensing of Environment 202: 18-27. doi:10.1016/j.rse.2017.06.031.
[20] Instituto de Investigaciones de la Amazonía Peruana (IIAP) and Gobierno Regional de Amazonas (GOREA) (2016): Zonificación ecológica y económica del departamento de Amazonas. – Zoonificacion Ecologica y Economica de Amazonas 15018: 1-23.
[21] Jin, Y. H., Liu, X. P., Chen, Y. M., Liang, X. (2018): Land-cover mapping using Random Forest classification and incorporating NDVI time-series and texture: a case study of central Shandong. – International Journal of Remote Sensing 39(23): 8703-8723. doi:10.1080/01431161.2018.1490976.
[22] Kah, M., Faye, C., Mbaye, M. L., Yalo, N., Gunnar, L. (2025): Hydroclimatic Trends and Land Use Changes in the Continental Part of the Gambia River Basin: Implications for Water Resources. – Water 17(14): 2075. https://doi.org/10.3390/w17142075.


http://www.aloki.hu ● ISSN 1589 1623 (Print) ● ISSN 1785 0037 (Online)
DOI: http://dx.doi.org/10.15666/aeer/2403_49654993
© 2026, ALÖKI Kft., Budapest, Hungary

[23] Kassaye, S. M., Tadesse, T., Tegegne, G., Hordofa, A. T., Malede, D. A. (2024): Relative and Combined Impacts of Climate and Land Use/Cover Change for the Streamflow Variability in the Baro River Basin (BRB). – Earth 5(2): 149-168. doi:10.3390/earth5020008.

[24] Liu, J., Li, M., Li, R., Shalamzari, M. J., Ren, Y., Silakhori, E. (2025): Comprehensive Assessment of Drought Susceptibility Using Predictive Modeling, Climate Change Projections, and Land Use Dynamics for Sustainable Management. – Land 14(2): 337. doi:10.3390/land14020337.

[25] Logan, T. A., Nicoll, J., Laurencelle, J., et al. (2014): Radiometrically Terrain Corrected ALOS PALSAR Data Available from the Alaska Satellite Facility. – NASA/ADS, AGU FALL MEETING. Available at: https://ui.adsabs.harvard.edu/abs/2014AGUFMIN33B3762L/abstract (Accessed: 25 April 2021).

[26] MINAM (Ministerio de Ambiente) (2015): Análisis de las Dinamicas de Cambio de Cobertura de la Tierra en la Comunidad Andina. – Ministerio del Ambiente, pp. 20-30. Available at: http://www.minam.gob.pe/ordenamientoterritorial/wp-content/uploads/sites/18/2013/10/Informe-final-de-Proyecto-Dinamica-de-los-Cambios-de-la-Tierra-CAN.pdf.

[27] MINAM (Ministerio del Ambiente) (2016a): Guía de uso y análisis de la información georreferenciada de bosques. – Ministerio del Ambiente. Available at: https://geo.serfor.gob.pe/geoserfor/images/Reporte_Bosques/GUIA_DE_USO_Y_ANALISIS_DE_LA_INFORMACION_GEORREFERENCIADA_DE_BOSQUES.pdf.

[28] MINAM (Ministerio del Ambiente) (2016b): Plan Nacional De Gestión Integral de Residuos Sólidos. – Ministerio del Ambiente. Available at: https://www.minam.gob.pe/calidadambiental/wp-content/uploads/sites/22/2013/10/IMPRIMIR-PLANRES-2016-2024-25-07-16.pdf.

[29] Moraes, D., Campagnolo, M. L., Caetano, M. (2024): Training data in satellite image classification for land cover mapping: a review. – European Journal of Remote Sensing 57(1). doi:10.1080/22797254.2024.2341414.

[30] MTC (Ministerio de Trasmportes y Comunicaciones) (2022): Descarga de Datos Espaciales-Transporte Terrestre por Carretera, en linea. – Available at: https://portal.mtc.gob.pe/estadisticas/descarga.html (Accessed: 23 July 2022).

[31] Organización de las Naciones Unidas para la Agricultura y la Alimentación-(FAO) (1996): Forest resources assessment 1990. Survey of tropical forest cover and study of change processes. – Forestry Paper, p. 149.

[32] Osorio, L. P., Mas, J-F., Guerra, F., Maass, M. (2015): Analysis and modeling of deforestation processes: a case study in the Coyuquilla River Basin. – Investigaciones Geográficas 88: 60-74. https://doi.org/10.14350/rig.43853.

[33] Parracciani, C., Gigante, D., Mutanga, O., Bonafoni, S., Vizzari, M. (2024): Land cover changes in grassland landscapes: combining enhanced Landsat data composition, LandTrendr, and machine learning classification in google earth engine with MLP-ANN scenario forecasting. – GIScience and Remote Sensing 61(1). doi:10.1080/15481603.2024.2302221.

[34] Phan, T., Kuch, V., Lehnert, L. W. (2020): Land cover classification using google earth engine and random forest classifier-the role of image composition. – Remote Sensing 12(15). doi:10.3390/RS12152411.

[35] Pizarro, S. E., Pricope, N. G., Vargas-Machuca, D., Huanca, O., Naupari, J. (2022): Mapping Land Cover Types for Highland Andean Ecosystems in Peru Using Google Earth Engine. – Remote Sensing 14(7): 1562. doi:10.3390/rs14071562.

[36] Pontius, R. G., Shusas, E., McEachern, M. (2004): Detecting important categorical land changes while accounting for persistence. – Agriculture, Ecosystems and Environment 101(2–3): 251-268. doi:10.1016/j.agee.2003.09.008.


http://www.aloki.hu ● ISSN 1589 1623 (Print) ● ISSN 1785 0037 (Online)
DOI: http://dx.doi.org/10.15666/aeer/2403_49654993
© 2026, ALÖKI Kft., Budapest, Hungary

[37] Rahaman, Z. A., Al Kafy, A., Saha, M., et al. (2022): Assessing the impacts of vegetation cover loss on surface temperature, urban heat island and carbon emission in Penang city, Malaysia. – Building and Environment 222: 109335. doi:10.1016/j.buildenv.2022.109335.
[38] Riaño, D., Chuvieco, E., Salas, J., Aguado, I. (2003): Assessment of different topographic corrections in landsat-TM data for mapping vegetation types (2003). – IEEE Transactions on Geoscience and Remote Sensing 41(5): 1056-1061. doi:10.1109/TGRS.2003.811693.
[39] Rodríguez-Echeverry, J., Echeverria, C., Oyarzún, C., Morales, L. (2018): Impact of land-use change on biodiversity and ecosystem services in the Chilean temperate forests. – Landscape Ecology 33(3): 439-453. doi:10.1007/s10980-018-0612-5.
[40] Rodriguez-Galiano, V. F., Ghimire, B., Rogan, J., Chica-Olmo, M., Rigol-Sanchez, J. P. (2012): An assessment of the effectiveness of a random forest classifier for land-cover classification. – ISPRS Journal of Photogrammetry and Remote Sensing 67: 93-104. doi:10.1016/j.isprsjprs.2011.11.002.
[41] Rojas Briceno, N. B., Barboza, E., Quintana, J. L. M., Oliva, M., Salas Lopez, R. (2019): Deforestación en la Amazonía peruana : índices de cambios de cobertura y uso del suelo basado en SIG Deforestation in the peruvian Amazon. – Boletín de la Asociación de Geógrafos Españoles.
[42] Schwamback, D., Amorim, B., Abderraman, R., et al. (2024): Land use transformations in the Brazilian Savanna: A decade of soil erosion and runoff measurements. – Catena 246: 108412. doi:10.1016/j.catena.2024.108412.
[43] Shiferaw, M., Kebebew, Z., Gemeda, D. O. (2023): Effect of forest cover change on ecosystem services in central highlands of Ethiopia: A case of Wof-Washa forest. – Heliyon 9(7): e18173. doi:10.1016/j.heliyon.2023.e18173.
[44] Srivastava, A., Chinnasamy, P. (2021): Investigating impact of land-use and land cover changes on hydro-ecological balance using GIS: insights from IIT Bombay, India. – SN Applied Sciences 3(3): 1-19. doi:10.1007/s42452-021-04328-7.
[45] Talukdar, S., Singha, P., Mahato, S., Shahfahad, Pal, S., Liou, Y.-A., Rahman, A. (2020): Land-use land-cover classification by machine learning classifiers for satellite observations: A review. – Remote Sensing 12(7): 1135. https://doi.org/10.3390/rs12071135.
[46] Tian, X., Consoli, D., Witjes, M., et al. (2025): Time series of Landsat-based bimonthly and annual spectral indices for continental Europe for 2000–2022. – Earth System Science Data 17(2): 741-772. doi:10.5194/essd-17-741-2025.
[47] Tiye, F. S., Korecha, D., Gutema, T. M., Gemeda, D. O. (2025): Modeling land use and land cover dynamics of Bale Mountains National Park using Google Earth Engine and cellular automata–artificial neural network (CA-ANN) model. – PLoS ONE 20(4): e0320428. doi:10.1371/journal.pone.0320428.
[48] Vargas, G. (1992): Análisis y clasificación del uso y cobertura de la tierra con interpretación de imágenes. – Instituto Geográfico Agustín Codazzi (IGAC), Bogotá.
[49] Wang, J., Bretz, M., Dewan, M. A. A., Delavar, M. A. (2022): Machine learning in modelling land-use and land cover-change (LULCC): Current status, challenges and prospects. – Science of the Total Environment 822: 153559. doi:10.1016/j.scitotenv.2022.153559.
[50] Wen, Z., Wang, Q., Ma, Y., et al. (2024): Remote estimates of suspended particulate matter in global lakes using machine learning models. – International Soil and Water Conservation Research 12(1): 200-216. doi:10.1016/j.iswcr.2023.07.002.
[51] World Bank (2022): Urban Development Overview, WorldBank. – Available at: https://www.worldbank.org/en/topic/urbandevelopment/overview (Accessed: 17 July 2025).
[52] van der Woude, S., Reiche, J., Sterck, F., Nabuurs, G-J., Vos, M., Herold, M. (2024): Sensitivity of Sentinel-1 Backscatter to Management-Related Disturbances in Temperate Forests. – Remote Sensing 16(9): 1553. doi:10.3390/rs16091553.


http://www.aloki.hu ● ISSN 1589 1623 (Print) ● ISSN 1785 0037 (Online)
DOI: http://dx.doi.org/10.15666/aeer/2403_49654993
© 2026, ALÖKI Kft., Budapest, Hungary

[53] Xia, J., Falco, N., Benediktsson, J. A., et al. (2017): Hyperspectral Image Classification with Rotation Random Forest Via KPCA. – IEEE Journal of Selected Topics in Applied Earth Observations and Remote Sensing 10(4): 1-9. 10.1109/JSTARS.2016.2636877.
[54] Yasin, E. H. E., Siddig, A. A. H., Diab, E. E., Czimber, K. (2025): Evaluating the Efficiency of Two Ecological Indices in Monitoring Forest Degradation in the Drylands of Sudan. – Remote Sensing 17(13): 1-19. doi:10.3390/rs17132298.
[55] Yin, L., Wang, L., Li, T., et al. (2023): U-Net-STN: A Novel End-to-End Lake Boundary Prediction Model. – Land 12(8): 1602. doi:10.3390/land12081602.
[56] Zafar, S. M., Khan, J. A., Mobeen, A., et al. (2025): Estimating the plausible projections of land use/land cover dynamics in Jhelum and Chenab River basins using satellite imageries and machine learning models in Google Earth Engine. – Geocarto International 40(1): 24. doi:10.1080/10106049.2025.2491640.
[57] Zhang, H. K., Luo, D., Roy, D. P. (2024): Improved Landsat Operational Land Imager (OLI) Cloud and Shadow Detection with the Learning Attention Network Algorithm (LANA). – Remote Sensing 16(8). doi:10.3390/rs16081321.


http://www.aloki.hu ● ISSN 1589 1623 (Print) ● ISSN 1785 0037 (Online)
DOI: http://dx.doi.org/10.15666/aeer/2403_49654993
© 2026, ALÖKI Kft., Budapest, Hungary

# APPENDIX

## *A.1 Spectral indices used in the classification and their mathematical formulations*

*Table A1* presents the spectral indices employed in this study, including their mathematical expressions and thematic relevance. These indices were used to enhance vegetation, moisture, and surface characteristics during the classification process.

***Table A1.*** *Spectral indices used and their mathematical formulas*

| Spectral Index | Formula | Description |
|---|---|---|
| NDVI | (NIR − RED) / (NIR + RED) | Normalized Difference Vegetation Index |
| EVI | 2.5 * ((NIR − RED) / (NIR + 6 * RED − 7.5 * BLUE + 1)) | Enhanced Vegetation Index |
| SAVI | (NIR − RED) / (NIR + RED + 0.5) * (1.5) | Soil-Adjusted Vegetation Index |
| NDWI | (NIR − SWIR) / (NIR + SWIR) | Normalized Difference Water Index |
| NBRI | (NIR - SWIR) / (NIR + SWIR) | Normalized Burn Ratio Index |
| GLI | (2 * GREEN - RED - BLUE) / (2 * GREEN + RED + BLUE) | Green Leaf Index |
| VARI | (GREEN - RED) / (GREEN + RED - BLUE) | Visible Atmospherically Resistant Index |
| GCI | (((NIR) / (GREEN)) - 1) | Green Chlorophyll Index |
| RGR | ((RED) / (GREEN)) | Red-Green Ratio |
| SIPI | ((NIR - BLUE) / (NIR - RED)) | Structure-Insensitive Pigment Index |
| ARVI | ((NIR - (2 * RED) + BLUE) / (NIR + (2 * RED) + BLUE)) | Atmospherically Resistant Vegetation Index |

## *A.2 Classification Accuracy Framework*

*Table A2* shows user and producer accuracy, as well as commission and omission errors by class.

***Table A2.*** *Confusion matrix structure based on Chuvieco (2007) and MINAM, (2015)*

| | | **Baseline results** | | | | | | |
|---|---|---|---|---|---|---|---|---|
| | | **Reference 1** | **Reference 2** | **…..** | **Reference n** | **Total** | **User accuracy** | **Commission error** |
| Ranking results | Class 1 | $a_{11}$ | $a_{12}$ | ….. | $a_{1n}$ | $a_{1+}$ | $a_{11} / a_{1+}$ | $1 - a_{11} / a_{1+}$ |
| | Class 2 | $a_{21}$ | $a_{22}$ | ….. | $a_{2n}$ | $a_{2+}$ | $a_{22} / a_{2+}$ | $1 - a_{22} / a_{2+}$ |
| | ….. | ….. | ….. | ….. | ….. | ….. | ….. | ….. |
| | Class n | $a_{n1}$ | $a_{n2}$ | ….. | $a_{nn}$ | $a_{n+}$ | $a_{nn} / a_{n+}$ | $1 - a_{nn} / a_{n+}$ |
| | Total | $a_{+1}$ | $a_{+2}$ | ….. | $a_{+n}$ | ***m*** | | |
| | Producer accuracy | $a_{11} / a_{+1}$ | $a_{22} / a_{+2}$ | ….. | $a_{nn} / a_{+n}$ | | | |
| | Error omission | $1 - a_{11} / a_{+1}$ | $1 - a_{22} / a_{+2}$ | ….. | $1 - a_{nn} / a_{+n}$ | | | |


http://www.aloki.hu ● ISSN 1589 1623 (Print) ● ISSN 1785 0037 (Online)
DOI: http://dx.doi.org/10.15666/aeer/2403_49654993
© 2026, ALÖKI Kft., Budapest, Hungary

### *A.3 LULC matrix*

*Table A3* includes the net change, total change, loss, gain, and exchange between two dates.

***Table A3.*** *Cross-tabulation matrix for land cover change between two dates, following FAO (1996) and Pontius et al. (2004)*

| **Date 1** | **Date 2** | | | | **Total date 1 ($P_{i+}$)** | **Loss ($L_i$)** | **Total change (Ct)** | **Net Change (Cn)** | **Interchange (Int)** |
|---|---|---|---|---|---|---|---|---|---|
| | **Class 1** | **Class 2** | **….** | **Class j** | | **(%)** | | | |
| **Class 1** | $P_{11}$ | $P_{12}$ | …. | $P_{1j}$ | $P_{1+}$ | $P_{1+} - P_{11}$ | L + G | Ct - Int | 2*min(L,G) |
| **Class 2** | $P_{21}$ | $P_{22}$ | …. | $P_{2j}$ | $P_{2+}$ | $P_{2+} - P_{22}$ | | | |
| **…..** | ….. | ….. | …. | ….. | ….. | ….. | | | |
| **Class i** | $P_{i1}$ | $P_{i2}$ | …. | $P_{ij}$ | $P_{i+}$ | $P_{i+} - P_{ij}$ | | | |
| **Total Date 2 ($P_{+j}$)** | $P_{+1}$ | $P_{+2}$ | …. | $P_{+j}$ | ***1*** | | | | |
| **Gain ($G_j$)** | $P_{+1} - P_{11}$ | $P_{+2} - P_{22}$ | …. | $P_{+j} - P_{ij}$ | | | | | |

### *A.4 Land use and land cover dynamics*

***Table A4.*** *Area (ha and %) and percentage change in land use/land cover classes in the Jucusbamba micro-basin during 1992, 2007, and 2022*

| **CCUS Classes** | **1992** | | **2007** | | **2022** | | **1992-2007** | **2007-2022** |
|---|---|---|---|---|---|---|---|---|
| | **ha** | **%** | **ha** | **%** | **ha** | **%** | **Δ %** | **Δ %** |
| **Forests-BO** | 7561.32 | 39.45 | 6956.17 | 36.29 | 5856.77 | 30.56 | -3.16 | -5.74 |
| **Mosaic of pastures and crops-PC** | 2270.83 | 11.85 | 3882.18 | 20.25 | 6939.96 | 36.21 | 8.41 | 15.95 |
| **Built-up areas-ZU** | 25.59 | 0.13 | 58.01 | 0.30 | 170.77 | 0.89 | 0.17 | 0.59 |
| **Shrub / herbaceous vegetationAH** | 9152.65 | 47.75 | 8112.08 | 42.32 | 6038.01 | 31.50 | -5.43 | -10.82 |
| **Herbazal/Pajonal-PH** | 156.92 | 0.82 | 158.87 | 0.83 | 161.80 | 0.84 | 0.01 | 0.02 |
| **Total** | 19167.31 | 100.00 | 19167.31 | 100.00 | 19167.31 | 100.00 | | |

### *A.5 Verification sampling for the 2022 CUS map*

***Table A5.*** *Distribution of verification points by land use/land cover class for the 2022 map*

| **Land cover and land use** | **COD** | **Area** | **Area %** | **Points/Verification** |
|---|---|---|---|---|
| **Forests** | BO | 5856.8 | 0.31 | 56 |
| **Mosaic of pastures and crops** | PC | 6940.0 | 0.36 | 63 |
| **Built-up areas** | ZU | 170.8 | 0.01 | 11 |
| **Shrub/herbaceous vegetation** | AH | 6038.0 | 0.32 | 56 |
| **Herbazal/Pajonal** | PH | 161.8 | 0.01 | 10 |
| **Total** | | 19167.3 | 1.00 | 196 |


http://www.aloki.hu ● ISSN 1589 1623 (Print) ● ISSN 1785 0037 (Online)
DOI: http://dx.doi.org/10.15666/aeer/2403_49654993
© 2026, ALÖKI Kft., Budapest, Hungary

### *A.6 Confusion matrix for the CUS 2022 map*

***Table A6.*** *Confusion matrix with user and producer accuracy, compromise*

| Baseline results | | | | | | | | | |
|---|---|---|---|---|---|---|---|---|---|
| | | **BO** | **PC** | **ZU** | **AH** | **PH** | **Total** | **User accuracy** | **Commission error** |
| **Ranking results** | **BO** | 51 | 4 | 0 | 2 | 0 | 57 | 0.89 | 0.11 |
| | **PC** | 3 | 58 | 0 | 2 | 0 | 63 | 0.92 | 0.08 |
| | **ZU** | 0 | 0 | 11 | 0 | 0 | 11 | 1.00 | 0.00 |
| | **AH** | 0 | 7 | 0 | 49 | 0 | 56 | 0.88 | 0.13 |
| | **PH** | 2 | 0 | 0 | 0 | 7 | 9 | 0.78 | 0.22 |
| | **Total** | 56 | 69 | 11 | 53 | 7 | 196 | | |
| | **Producer accuracy** | 0.91 | 0.84 | 1.00 | 0.92 | 1.00 | Overall Accuracy = 89.8% | | |
| | **Error omission** | 0.09 | 0.16 | 0.00 | 0.08 | 0.00 | Kappa Index = 0.86 | | |

### *A.7 Land cover change matrix: 1992–2007*

***Table A7.*** *Cross-tabulation matrix and rate of change for the period 1992–2007*

| **1992** | **2007** | | | | | **Total 1992** | **Exchange rate** | **Loss ($L_i$)** | **Total change (Ct)** | **Net Change (Cn)** | **Interchange (Int)** |
|---|---|---|---|---|---|---|---|---|---|---|---|
| | **BO** | **PC** | **ZU** | **AH** | **PH** | **%** | | | | | |
| **BO** | 6956.17 | 601.97 | 1.23 | 0.00 | 1.95 | 7561.32 | -0.55 | 8.00 | 8.00 | 8.00 | 0.00 |
| **PC** | 0.00 | 2246.57 | 24.257 | 0.00 | 0.00 | 2270.83 | 3.64 | 1.07 | 73.09 | 70.96 | 2.14 |
| **ZU** | 0.00 | 0.00 | 25.588 | 0.00 | 0.00 | 25.59 | 5.61 | 0.00 | 126.69 | 126.69 | 0.00 |
| **AH** | 0.00 | 1033.63 | 6.9364 | 8112.08 | 0.00 | 9152.65 | -0.80 | 11.37 | 11.37 | 11.37 | 0.00 |
| **PH** | 0.00 | 0.00 | 0.00 | 0.00 | 156.9246 | 156.92 | 0.08 | 0.00 | 1.24 | 1.24 | 0.00 |
| **Total 2007** | 6956.17 | 3882.18 | 58.01 | 8112.08 | 158.87 | 19167.31 | | | | | |
| **Gain ($G_j$) (%)** | 0.00 | 72.03 | 126.69 | 0.00 | 1.24 | | | | | | |

### *A.8 Land cover change matrix: 2007–2022*

***Table A8.*** *Cross-tabulation matrix and rate of change for the period 2007–2022*

| **2007** | **2022** | | | | | **Total 2007** | **Exchange rate** | **Loss ($L_i$)** | **Total change (Ct)** | **Net Change (Cn)** | **Interchange (Int)** |
|---|---|---|---|---|---|---|---|---|---|---|---|
| | **BO** | **PC** | **ZU** | **AH** | **PH** | **%** | | | | | |
| **BO** | 5856.8 | 651.8 | 0.4 | 444.3 | 2.9 | 6956.17 | -1.14 | 15.80 | 15.80 | 15.80 | 0.00 |
| **PC** | 0 | 3808.2 | 74.0 | 0 | 0 | 3882.18 | 3.95 | 1.91 | 82.58 | 78.76 | 3.81 |
| **ZU** | 0 | 0 | 58.0 | 0 | 0 | 58.01 | 7.46 | 0.00 | 194.40 | 194.39 | 0.01 |
| **AH** | 0 | 2480.0 | 38.3 | 5593.7 | 0 | 8112.08 | -1.95 | 31.04 | 36.52 | 25.57 | 10.95 |
| **PH** | 0 | 0 | 0 | 0 | 158.9 | 158.87 | 0.12 | 0.00 | 1.84 | 1.84 | 0.00 |
| **Total 2022** | 5856.77 | 6939.96 | 170.77 | 6038.01 | 161.80 | **19167.31** | | | | | |
| **Gain ($G_j$) (%)** | 0.00 | 80.67 | 194.39 | 5.48 | 1.84 | | | | | | |


http://www.aloki.hu ● ISSN 1589 1623 (Print) ● ISSN 1785 0037 (Online)
DOI: http://dx.doi.org/10.15666/aeer/2403_49654993
© 2026, ALÖKI Kft., Budapest, Hungary

### *A.9 Forest loss intensity (1992–2022)*

***Table A9.*** *Forest loss area and annual intensity concentration (low to extremely high) for 1992–2007 and 2007–2022*

| Loss of Forests/ ha | Concentration/year | 1992-2007 | 2007-2022 |
|---|---|---|---|
| Non-accumulated area | Low | 12137.84 | 8737.13 |
| | Media | 4019.28 | 4605.03 |
| | High | 2024.23 | 3193.36 |
| | Very high | 721.04 | 1878.31 |
| | Extremely high | 264.89 | 753.46 |
| | **Total** | **19167.28** | **19167.28** |
| | Low | 63.33% | 45.58% |
| | Media | 20.97% | 24.03% |
| | High | 10.56% | 16.66% |
| | Very high | 3.76% | 9.80% |
| | Extremely high | 1.38% | 3.93% |
| | **Total** | **100.00%** | **100.00%** |
| Accumulated area | Low | 19167.28 | 19167.28 |
| | Media | 7029.44 | 10430.15 |
| | High | 3010.16 | 5825.12 |
| | Very high | 985.93 | 2631.77 |
| | Extremely high | 264.89 | 753.46 |
| | **Total** | **100.00%** | **100.00%** |
| | Low | 62.93 | 49.39 |
| | Media | 23.08 | 26.88 |
| | High | 9.88 | 15.01 |
| | Very high | 3.24 | 6.78 |
| | Extremely high | 0.87 | 1.94 |

### *A.10 Projected change in land cover: 2022–2037*

***Table A10.*** *Cross-tabulation matrix and projected rate of change for 2022–2037*

| 2022 | 2037 | | | | | Total 2022 | Exchange rate | Loss ($L_i$) | Total change (Ct) | Net Change (Cn) | Interchange (Int) |
|---|---|---|---|---|---|---|---|---|---|---|---|
| | BO | PC | ZU | AH | PH | % | | | | | |
| **BO** | 5716.5 | 94.5 | 0.2 | 42.2 | 3.4 | 5856.77 | -0.16 | 2.40 | 2.40 | 2.40 | 0.00 |
| **PC** | 0 | 6890.9 | 9.3 | 39.7 | 0 | 6939.96 | 0.44 | 0.71 | 8.18 | 6.77 | 1.41 |
| **ZU** | 0 | 0 | 170.8 | 0 | 0 | 170.77 | 0.37 | 0.00 | 5.68 | 5.68 | 0.00 |
| **AH** | 0 | 421.0 | 0.2 | 5616.7 | 0.1 | 6038.01 | -0.38 | 6.98 | 8.34 | 5.62 | 2.72 |
| **PH** | 0 | 3.0 | 0 | 0.1 | 158.7 | 161.80 | 0.02 | 1.89 | 4.02 | 3.99 | 0.03 |
| **Total 2037** | 5716.4 | 7409.4 | 180.4 | 6598.7 | 2162.2 | **19167.31** | | | | | |
| **Gain ($G_j$) (%)** | 0.00 | 7.47 | 5.68 | 1.36 | 2.13 | | | | | | |


http://www.aloki.hu ● ISSN 1589 1623 (Print) ● ISSN 1785 0037 (Online)
DOI: http://dx.doi.org/10.15666/aeer/2403_49654993
© 2026, ALÖKI Kft., Budapest, Hungary

### *A.11 Projected change in land cover: 2037–2052*

***Table A11.*** *Cross-tabulation matrix and projected rate of change for 2037–2052*

| 2037 | 2052 | | | | | Total 2037 | Exchange rate | Loss ($L_i$) | Total change (Ct) | Net Change (Cn) | Interchange (Int) |
|---|---|---|---|---|---|---|---|---|---|---|---|
| | BO | PC | ZU | AH | PH | % | | | | | |
| **BO** | 5575.1 | 120.3 | 0.2 | 19.4 | 1.6 | 5716.46 | -0.17 | 2.47 | 2.47 | 2.47 | 0.00 |
| **PC** | 0 | 7404.6 | 4.0 | 0.8 | 0.1 | 7409.48 | 0.38 | 0.07 | 6.06 | 5.92 | 0.13 |
| **ZU** | 0 | 0 | 180.46 | 0 | 0 | 180.46 | 0.16 | 0.00 | 2.37 | 2.37 | 0.00 |
| **AH** | 0 | 322.3 | 0.1 | 5376.3 | 0 | 5698.72 | -0.36 | 5.66 | 6.01 | 5.30 | 0.71 |
| **PH** | 0 | 1.3 | 0 | 0 | 160.9 | 162.20 | 0.01 | 0.80 | 1.81 | 1.79 | 0.03 |
| **Total 2052** | 5575.09 | 7848.45 | 184.75 | 5396.49 | 162.53 | 19167.31 | | | | | |
| **Gain ($G_j$) (%)** | 0.00 | 5.99 | 2.37 | 0.35 | 1.01 | | | | | | |

### *A.12 Projected intensity of forest loss (2022–2052)*

***Table A12.*** *Projections of forest area loss and annual intensity concentration for 2022–2037 and 2037–2052*

| Forest Loss/ha | Concentration/year | 2022-2037 | 2037-2052 |
|---|---|---|---|
| **Non-accumulated area** | Low | 9594.83 | 11758.36 |
| | Media | 3685.05 | 3389.22 |
| | High | 2962.14 | 2443.66 |
| | Very high | 2028.16 | 1127.64 |
| | Extremely high | 897.10 | 448.40 |
| | **Total** | 19167.28 | 19167.28 |
| | Low | 50.06% | 61.35% |
| | Media | 19.23% | 17.68% |
| | High | 15.45% | 12.75% |
| | Very high | 10.58% | 5.88% |
| | Extremely high | 4.68% | 2.34% |
| | **Total** | 100.00% | 100.00% |
| **Accumulated area** | Low | 19167.28 | 19167.28 |
| | Media | 9572.45 | 7408.92 |
| | High | 5887.41 | 4019.70 |
| | Very high | 2925.26 | 1576.04 |
| | Extremely high | 897.10 | 448.40 |
| | **Total** | **100.00%** | **100.00%** |
| | Low | 49.85 | 58.76 |
| | Media | 24.90 | 22.71 |
| | High | 15.31 | 12.32 |
| | Very high | 7.61 | 4.83 |
| | Extremely high | 2.33 | 1.37 |


http://www.aloki.hu ● ISSN 1589 1623 (Print) ● ISSN 1785 0037 (Online)
DOI: http://dx.doi.org/10.15666/aeer/2403_49654993
© 2026, ALÖKI Kft., Budapest, Hungary